

Evaluating the maximum drilling length of horizontal geothermal wells utilizing temperature constraints



Xi Wang ^{a,b}, Feifei Zhang ^{a,b,*}, Xueying Wang ^{a,b}, Yibin Yu ^{a,b}, Wenqiang Lou ^{a,b}, Fengjia Peng ^{a,b}

^a Hubei Key Laboratory of Oil and Gas Drilling and Production Engineering (Yangtze University), Hubei Province, Wuhan 430100, China

^b School of Petroleum Engineering, Yangtze University: National Engineering Research Center for Oil & Gas Drilling and Completion Technology, Wuhan 430100, China

ABSTRACT

The geothermal industry faces a significant challenge in exploring and developing resources due to elevated temperatures in downhole environments. Successful drilling in high-temperature geothermal wells requires precise thermal management. This research assesses constraints on horizontal section length and temperature during geothermal horizontal well drilling, aiming to formulate effective wellbore temperature management guidelines.

The study utilizes thermal resistance analysis to establish a tailored transient heat transfer model for high-temperature horizontal geothermal well drilling. Parameters such as circulation time, horizontal section length, flow rate, drilling fluid properties, formation thermal conductivity, and drill string thermal conductivity are thoroughly investigated. Treating input parameters as triangular distributions, Monte Carlo simulation techniques conduct sensitivity analysis. Tornado diagrams quantitatively determine key parameter impacts on bottom-hole temperature. The research introduces a procedural framework for geothermal well drilling, aiding engineers in swiftly identifying operational parameter combinations for effective wellbore temperature management. This workflow provides practical guidance for geothermal resource development, ensuring drilling safety in diverse conditions.

1. Introduction

Geothermal energy is an important clean and sustainable energy source because it offers numerous environmental, economic, and social benefits. There are two major approaches to utilize geothermal energy, electric power generation and direct use for heating or cooling. The key point of the efficient and economical geothermal development is the sustainable heat exchange rate for the range of project life time. Studies show that only 10% of the estimated global potential has been developed (Queslati et al., 2019). One of the major constraints for these unrecovered geothermal resources are unsustainable or insufficient heat exchange rate. There are three major approaches to extract heat from underground, circulation through single well, circulation through wells connected by fractures (including both natural fractures and induced fractures), and circulation through intersected wells. For all of these three types, heat exchange rate can be increased by increasing the contact area, which can be achieved by drilling long horizontal wells in geothermal reservoir. Well construction has been one of the most challenging chapters during geothermal development. Statistics show that drilling and well construction typically account for 50–75% of cost for the entire geothermal projects (Feder, 2021).

Geothermal energy plays a pivotal role in the global pursuit of sustainable and clean energy alternatives. This inevitably leads to

fundamental differences between geothermal drilling and traditional oil and gas (O&G) drilling. Whereas O&G drilling is primarily aimed at extracting hydrocarbons, geothermal drilling seeks to harness subsurface thermal energy. This divergence in core objectives necessitates variations in drilling techniques and technological applications. Geothermal drilling faces more severe challenges compared to conventional O&G drilling, one reason being the high-temperature conditions of its operational environment. This environment demands that drilling tools and technologies withstand extreme thermal challenges, including the thermal limitations of directional drilling tools, the temperature resilience of electronic components in measurement-while-drilling (MWD) tools, and the high-temperature and corrosion resistance of drilling fluids (Mohamed et al., 2017; Pastorek et al., 2019). A significant issue is that most downhole sensors and measurement tools are designed to function only up to a maximum temperature of 175 °C, yet temperatures in geothermal formations often exceed this range, reaching or surpassing 200 °C (Tomac and Sauter, 2017; Liu and Gao, 2017). Additionally, traditional mud motors and rotary steerable systems (RSS), as well as drilling fluids, have limited high-temperature capabilities, which are inadequate for the demands of geothermal drilling (Mohamed et al., 2021). Despite these challenges, there are substantial synergistic opportunities between geothermal and O&G drilling. The O&G industry has accumulated extensive experience and advanced

* Corresponding author.

E-mail address: feifei-zhang@yangtzeu.edu.cn (F. Zhang).

technology in areas such as directional drilling, hydraulic fracturing, and digital well monitoring (Ma et al., 2016; Moska et al., 2021; Osinde et al., 2019). These technologies can offer invaluable support for the precise exploration and efficient extraction of geothermal resources. For instance, leveraging directional drilling technology from the O&G industry can enhance the precision with which geothermal resources are accessed, thereby improving extraction efficiency. The application of hydraulic fracturing could play a significant role in the development of geothermal resources by creating denser underground well networks that enhance heat exchange efficiency. Furthermore, the application of digital well technology can facilitate real-time monitoring and optimization of geothermal drilling operations, helping to reduce costs and minimize risks. On the other hand, the experience and technological advancements in the geothermal drilling sector also offer valuable insights for the O&G industry. The adoption of high-temperature drill bits and sensor technologies can aid the O&G sector in better managing the high-pressure and high-temperature conditions encountered in deep-water and ultra-deep drilling, enhancing safety and efficiency (Pastorek et al., 2019; Song et al., 2023). Thus, through technological exchange and collaboration, both the geothermal and O&G industries can mutually benefit, driving innovation and development in the energy sector towards the common goal of sustainable energy solutions.

Compared to O&G reservoirs, understanding and characterizing geothermal reservoirs presents unique challenges. Geothermal reservoirs involve complex geological structures with diverse heat transfer mechanisms, making accurate reservoir characterization and modeling critical (Cao et al., 2024). A number of studies have been conducted to develop thermal models and estimate the downhole temperature (DHT) while drilling. The field of heat transfer modeling employs two main methods: analytical models and numerical models (Yang et al., 2019). Analytical models are built upon heat transfer theory and thermodynamic principles, utilizing mathematical formulas to quantitatively describe heat transfer behavior in wellbores under various conditions. The exploration of wellbore temperature dates back to the 1940s (Farris, 1941), but the development of analytical models specifically for wellbore temperature began in the early 1960s. Edwardson et al. (1962) assumed a constant wellbore wall temperature or a constant heat rate and employed an implicit function to describe the temperature drop per unit area in the rock formation, thereby establishing an analytical model for wellbore heat transfer. Ramey (1962), on the other hand, formulated a temperature prediction model for single-phase fluids based on the assumption of steady-state heat transfer within the wellbore and transient heat transfer in the surrounding formation. These studies laid foundation for subsequent research and the evolution of analytical models for wellbore heat transfer. Holmes and Swift (1970) developed a mathematical model that predicts the temperature of drilling mud in the drill string and annulus during drilling at any depth. Keller et al. (1973) proposed a model to describe the two-dimensional heat transfer phenomena inside and around the wellbore. Influenced by Edwardson's viewpoint, their model treated heat transfer within the drill string and annular fluid as steady-state and approximated the heat transfer between the annular fluid and the formation as steady-state linear heat transfer. Heat convection and conduction constitute the primary forms of heat exchange between the drilling fluid and the surrounding formation (Paredes, 2001; Song and Guan, 2011). The intricate heat transfer mechanisms result in non-steady-state heat interaction between the wellbore and the formation. Hasan and Kabir (Hasan et al., 2005; Hasan and Kabir, 1994a,b, 2012; Kabir et al., 1996) improved upon Ramey's model and proposed two-phase flow heat transfer models within the wellbore, considering transient heat transfer in the formation and steady-state heat transfer in the wellbore. This approach became the fundamental premise for the development of most subsequent analytical models. Researchers thereafter developed corresponding wellbore temperature prediction models for various conditions, including oil and gas production (Kutasov et al., 1988; Gao and Jalali, 2005), geothermal exploitation (Sun et al., 2017), water injection (Pimenov et al., 2005;

Yoshioka et al., 2007), fracturing (Yoshida et al., 2014), acidification (Tabatabaei et al., 2013), cementing (Saedi et al., 2018), and well shut-in (Saedi et al., 2019). However, due to the complexity of solving coupled physical models, these models often overlook the influence of factors such as complex casing structures, heat sources, and temperature-dependent thermal properties on the distribution of wellbore temperature, thereby limiting the accuracy of their predictive results. In contrast, numerical models have the ability to consider various influencing factors, such as multiple heat transfer mechanisms, flow conditions, and boundary conditions, in the wellbore heat transfer process. As a result, numerical models have found extensive use in predicting wellbore temperature and formation temperature distribution after altering injection parameters and operating conditions (Espinosa-Paredes et al., 2001; Yang et al., 2017). Raymond (1969) introduced the first numerical heat transfer model to predict wellbore temperature during vertical well circulation. Subsequent scholars improved upon this model by considering the coupled heat transfer mechanisms between different controlling regions of the wellbore and the formation, developing transient heat transfer models for wellbores in one dimension and formations in two dimensions (Ziabakhsh-Ganjiani et al., 2018). Typically, these models are solved using finite difference methods (FDM) and finite element methods (FEM). These studies investigated the effects of frictional heat (Keller et al., 1973; Kuthu et al., 2017), drill string rotation (Kårstad and Aadnøy, 1999; Kamel et al., 2017), drill string composition and geometry (Yang et al., 2017; Sui et al., 2018), formation influx and losses (Li et al., 2016; Zhang et al., 2019), groundwater flow rate (Hu, 2017), various fluid types (Chen and Novotny, 2003), as well as the circulation and cessation of the drilling process (Espinosa-Paredes and Garcia-Gutierrez, 2004) on the distribution of wellbore temperature. These studies have contributed to the enrichment and expansion of the application scope of transient heat transfer models.

The distinction in heat transfer during drilling horizontal and vertical wells primarily resides in the dissimilar temperature distributions and contact conditions existing between the vertical and horizontal sections formation. In horizontal section, while the formation temperature remains constant with respect to well depth, the elongated horizontal interval results in prolonged contact duration between the wellbore and the high-temperature formation. As well depth increases, the circulating drilling fluid spends more time within the wellbore, and the key factors influencing DHT, such as inlet temperature, thermal conductivity of the drill pipe, circulation time, circulation velocity, and drilling fluid properties, exert diminished influence. Consequently, drilling fluid temperature is more prone to reaching elevated temperature conditions (Trichel and Fabian, 2011; Khaled et al., 2023). Hence, the effective management of temperatures assumes heightened significance when drilling geothermal horizontal wells. To address the challenges associated with temperature management in high-temperature downhole environments, various techniques have been proposed. These include the utilization of insulating drill pipes, surface cooling devices, drilling fluid systems and additives possessing high heat capacity, as well as optimized construction parameters (Finger et al., 2000; Champness et al., 2008; Hickson et al., 2020; Xiao et al., 2022a). In their work, Khaled et al. (2023) assessed the efficacy of different temperature management techniques in geothermal wells. Their findings revealed that the implementation of surface mud cooling devices, specific drilling fluid systems, and higher flow rates can effectively reduce the circulating temperature at the bottomhole in shallow geothermal wells. Nevertheless, for deep geothermal wells and extensive horizontal sections, the cooling effect achieved through mud cooling and certain widely accepted temperature management measures is not substantial. Moreover, considering the influence of cost and efficiency factors during drilling operations, adjusting process parameters and drilling fluid systems may not be suitable for effective temperature management (Xiao et al., 2022a). When drilling geothermal horizontal wells, the combination of conventional drill pipes with insulated drill pipes can offer

sufficient cooling capabilities (Ando and Naganawa, 2020; Khaled et al., 2023). Furthermore, Khaled et al. (2023) presented drilling heat maps in his study to assist field engineers in rapidly comprehending the impact of diverse downhole cooling strategies on geothermal well drilling. These investigations have enriched and expanded the application scope of transient heat transfer models, while advanced optimization algorithms have been employed to streamline solution process and enhance computational stability.

In previous research, the academic and industrial focus regarding the heat transfer and control during drilling primarily centered on the development of heat transfer models and the analysis of specific cases. However, there is currently a lack of a systematic method within the industry for assessing the effectiveness of temperature limitations during drilling in geothermal formations, particularly for horizontal wells. A significant challenge arises due to the effects of high temperatures on traditional drilling fluids and downhole tools in horizontal drilling sections. These conditions can lead to the failure of downhole measurement tools, such as MWD systems, when exposed to prolonged high temperatures. Consequently, the tools and fluids used in the drilling process must operate within a specific temperature range, necessitating effective temperature control to ensure both the efficiency and safety of the drilling operations.

To address these challenges, the industry has developed several innovative materials and tools. These advancements include the use of phase change materials to enhance the specific heat capacity of drilling fluids (Xiao et al., 2022b), ground cooling systems to reduce the inlet temperature of drilling fluids (Angisani et al., 2016), insulated drill pipes to decrease thermal conductivity (Xiao et al., 2022a), and the creation of downhole tools made from high-temperature composite materials to withstand elevated temperatures (Cao et al., 2024). These innovations, combined with traditional thermal management techniques such as optimizing flow rates and extending circulation times, have culminated in the formation of a closed-loop wellbore temperature control system. This system ensures that both the drilling fluids and tools operate within a safe working temperature range.

Despite these developments, the new materials and methods have their own temperature limitations. In geothermal drilling, extending the length of the horizontal sections can enhance the heat exchange rate, but this improvement might also mitigate the effectiveness of the thermal management strategies. Theoretically, there exists a critical length; once surpassed, any cooling measures may become ineffective, causing wellbore temperatures to exceed the tolerance limits of all tools and materials involved, thereby hindering further drilling progress. Therefore, developing and implementing effective thermal management strategies is crucial for the success of geothermal drilling operations.

In this work, we propose a methodology to evaluate the length and temperature limits for drilling horizontal wells in geothermal formation. The purpose of this study is to investigate the applicability and effectiveness of different heat management techniques required to drill horizontal geothermal wells and provide guidelines for well design and cooling methods selection. Firstly, the major impact factors for geothermal drilling are analyzed by using a transient wellbore heat transfer model. Then, sensitivity analysis is performed on major impact factors to obtain a tornado map for these factors. At the end, a workflow to geothermal drilling analysis. Illustration of the workflow is shown by using cases from practical projects.

2. Thermal models

2.1. Basic assumptions

During the process of drilling, the injection of drilling fluid with a lower temperature takes place at the surface, specifically into the drill string. Subsequently, the fluid proceeds downwards along the drill string and reaches the annulus through the drill bit nozzles. Upon reaching the annulus, the fluid undergoes circulation back to the surface, thereby

concluding one complete circulation cycle, as depicted in Fig. 1. The differentiation between the blue and red arrows depicted in Fig. 1 pertains to their respective temperature characteristics, where the red hue signifies a relatively elevated temperature, while the blue hue signifies a relatively reduced temperature. Moreover, the small red arrows delineate the directionality of heat transfer. Here, 'z' represents the direction of the wellbore axis, 'r' denotes the direction perpendicular to the wellbore axis, with the arrow direction considered as positive.

Throughout the drilling of geothermal wells, a complex interplay of heat exchange phenomena manifests between various segments of the wellbore and the encompassing formation. All heat transfer mechanisms are regarded as transient in nature. Frictional heat sources may be locally accounted for at each segment. Consequently, the temperature of the drilling fluid experiences temporal variations both within the drill string and within the annulus. The ensuing assumptions serve as foundational premises for modeling the dynamic thermal transfer process along the wellbore.

- (1) The thermal energy generated by the circulating frictional resistance of drilling fluid within the drill string and annulus is negligible;
- (2) Phase changes or fluid losses are not considered in the model;
- (3) Surrounding rocks are presumed to have isotropic thermal properties;
- (4) The influence of drilling fluid rotation on heat transfer is disregarded;
- (5) It is postulated that the pore fluid exhibits Newtonian characteristics, and the flow within the formation is confined solely to the radial direction.

2.2. Governing equation

In order to derive the governing equations for the thermal variations of drilling fluid within the wellbore during its flow, the wellbore is discretized into multiple controlled volumes along the z-direction, each of uniform length dZ . Illustrated in Fig. 2 is a control volume featuring heat fluxes entering and exiting the element. Fig. 2(a) represents the control volume inside the drill string, while Fig. 2(b) depicts the control volume in the annulus. The drilling fluid inside the drill string and in the annulus are studied separately. The detailed derivation process of the mathematical formulation for the thermal model is presented as follows:

2.2.1. Heat transfer model inside the drill string

(1) As the fluid traverses down the drill string along the z-direction, the heat (dQ_p^e) conveyed into the volume element during the time interval dt is represented as follows:

$$dQ_p^e = Q_p(Z, t) - Q_p(Z + dZ, t) = \rho_p Q c_p [T_p(Z, t) - T_p(Z + dZ, t)] dt \quad (1)$$

Where $Q_p(Z, t)$ is the heat at the upper portion of the drill string volume element at time t ; $Q_p(Z + dZ, t)$ is the heat at the lower portion of the drill string volume element at time t ; ρ_p is the density of the drilling fluid within the drill string, kg/m^3 ; Q is flow rate, m^3/s ; c_p is the specific heat capacity of the drilling fluid within the drill string, $\text{J}/(\text{kg}\cdot\text{K})$; $T_p(Z, t)$ is the temperature at the upper portion of the drilling fluid within the drill string volume element at time t , K ; $T_p(Z + dZ, t)$ is the temperature at the lower portion of the drilling fluid within the drill string volume element at time t , K .

(2) The convective heat transfer occurring between the fluid within the drill string and the interior surface of the drill string (dQ_p^r) is formally defined as:

$$dQ_p^r = Q_{a-p}(Z, t) = \frac{T_a(Z, t) - T_p(Z, t)}{R_{pa}} dZ dt \quad (2)$$

Where $Q_{a-p}(Z, t)$ is the convective heat transfer occurring between the

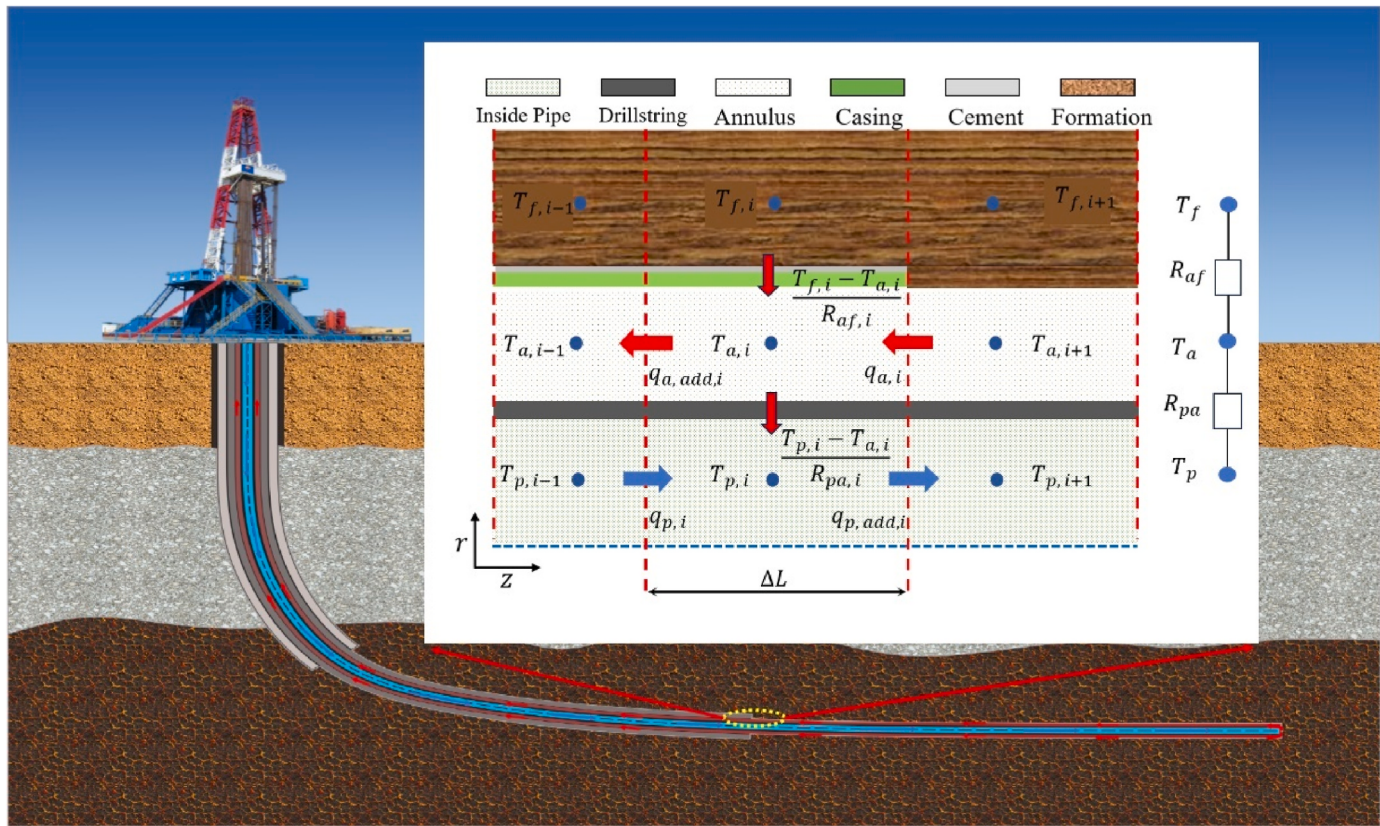


Fig. 1. Schematic of heat transfer process in geothermal wells.

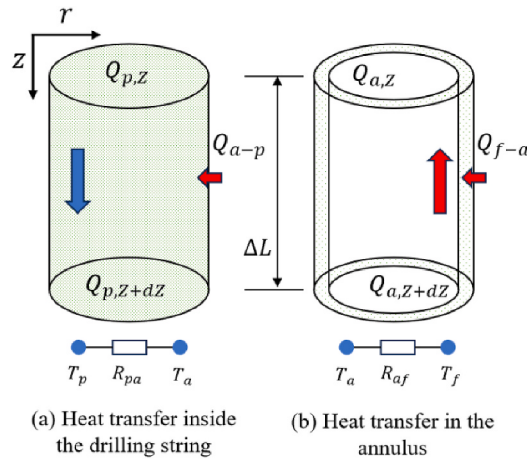


Fig. 2. Schematic of heat transfer process in control volume.

drilling fluid within the drill string and the interior surface of the drill string at time t in the upper portion of the volume element, J ; $T_a(Z, t)$ is the temperature of the drilling fluid in the annulus at the upper portion of the volume element at time t , K; R_{pa} is the thermal resistance of the drill string, which is related to the convective heat transfer resistance between the inner and outer walls of the drill string and the drilling fluid, (K·m)/W.

(3) The accumulation of energy within the volume element of fluid in the drill string (dE_p) is depicted as:

$$dE_p = \frac{\pi D_{pi}^2}{4} dZ \frac{\partial(c_p \rho_p T_p)}{\partial t} dt \quad (3)$$

Where D_{pi} is the inner diameter of the drill string, m.

(4) The thermal power per unit length generated by other conditions (such as fluid friction and drill string rotation) is defined as W_p , expressed as:

$$dW_p = q_{p, add} dZ dt \quad (4)$$

Where $q_{p, add}$ is the additional heat source term inside the drill string, W/m.

According to the law of energy conservation, the heat entering the control body minus the heat leaving the control body equals the internal energy change of the control body. The conservation of energy inside the drill string can be expressed by Equation (5):

$$\begin{aligned} \frac{\pi D_{pi}^2}{4} dZ \frac{\partial(c_p \rho_p T_p)}{\partial t} dt &= \rho_p Q c_p [T_p(Z, t) - T_p(Z + dZ, t)] dt + \frac{T_a - T_p}{R_{pa}} dZ dt \\ &+ q_{p, add} dZ dt \end{aligned} \quad (5)$$

Both sides of the equation were divided by $dZ dt$:

$$\frac{\pi D_{pi}^2}{4} \frac{\partial(c_p \rho_p T_p)}{\partial t} = \frac{T_a - T_p}{R_{pa}} - \rho_p Q \frac{\partial(c_p T_p)}{\partial Z} + q_{p, add} \quad (6)$$

2.2.2. Heat transfer model in the annulus

(1) As the fluid flows upward through the annulus along the z -direction, the heat (dQ_a^c) carried into the volume element during the time interval dt is expressed as:

$$dQ_a^c = Q_a(Z, t) - Q_a(Z + dZ, t) = -\rho_a Q c_a [T_a(Z, t) - T_a(Z + dZ, t)] dt \quad (7)$$

Where $Q_a(Z, t)$ is the heat at the upper portion of the annular volume element at time t , J; $Q_a(Z + dZ, t)$ is the heat at the lower portion of the annular volume element at time t , J; c_a is the specific heat capacity of the drilling fluid within the annulus, J/(kg·K); ρ_a is the density of the drilling fluid within the annulus, kg/m³; $T_a(Z, t)$ is the temperature at the upper

portion of the drilling fluid within the annulus volume element at time t , K; $T_a(Z+dZ, t)$ is the temperature at the lower portion of the drilling fluid within the annulus volume element at time t , K.

(2) The convective heat transfer occurring between the exterior wall of the drill string and the fluid within the annulus, as well as between the wellbore wall and the annulus fluid, is formally expressed as (dQ_a^r):

$$dQ_a^r = Q_{f-a}(Z, t) + Q_{a-p}(Z, t) = \frac{T_f - T_a}{R_{af}} dZ dt - \frac{T_a - T_p}{R_{pa}} dZ dt \quad (8)$$

Where $Q_{f-a}(Z, t)$ is the convective heat transfer occurring between the wellbore wall and the annulus fluid at time t in the upper portion of the volume element, J; T_f is formation temperature, K; R_{af} is the thermal resistance of the annulus, which is related to the convective heat transfer resistance between the drilling fluid in the annulus and the wellbore, the thermal resistance between the casing and the cement sheath (considered only in the cased section, ignored in the open hole section), and the thermal resistance of the formation, (K·m)/W.

(3) The accumulation of energy within the volume element of fluid in the annulus (dE_a) is depicted as:

$$dE_a = \frac{\pi(D_{ai}^2 - D_{po}^2)}{4} dZ \frac{\partial(c_a \rho_a T_a)}{\partial t} dt \quad (9)$$

Where D_{ai} is the diameter of the annulus, m; D_{po} is the outer diameter of the drill string, m.

(4) The rotation of the drill string and fluid friction also generate heat, represented as:

$$dW_a = q_{a,add} dZ dt \quad (10)$$

Where $q_{a,add}$ is additional heat source term inside the annulus, W/m.

Similarly, in accordance with the law of energy conservation, the conservation of energy in the annulus can be expressed by Equation

$$\begin{aligned} \frac{\pi(D_{ai}^2 - D_{po}^2)}{4} dZ \frac{\partial(c_a \rho_a T_a)}{\partial t} dt &= \rho_a Q c_a [T_a(Z+dZ, t) - T_a(Z, t)] dt + \left(\frac{T_f - T_a}{R_{af}} \right. \\ &\quad \left. - \frac{T_a - T_p}{R_{ap}} \right) dZ dt + q_{a,add} dZ dt \end{aligned} \quad (11)$$

Similarly, this can be simplified to:

$$\frac{\pi(D_{ai}^2 - D_{po}^2)}{4} \frac{\partial(c_a \rho_a T_a)}{\partial t} = \rho_a Q \frac{\partial(c_a T_a)}{\partial L} + \frac{T_f - T_a}{R_{af}} - \frac{T_a - T_p}{R_{ap}} + q_{a,add} \quad (12)$$

2.2.3. Heat transfer models of wellbore wall and formation

In consideration of the influence of the formation's porous fluid, the heat transfer processes in the vicinity of the wellbore strata encompass both radial and axial heat conduction, along with convective heat transfer of the fluid. The temperature distribution in the near-wellbore strata can be determined through the employment of the diffusion equation, as follows:

$$\frac{\rho_f c_f}{\lambda_{for}} \frac{\partial T_f}{\partial t} + \left(\frac{\rho_{pf} c_{pf}}{\lambda_{for}} \right) v_r \frac{\partial T_f}{\partial r} = \frac{\partial^2 T_f}{\partial r^2} + \frac{1}{r} \frac{\partial T_f}{\partial r} + \frac{\partial^2 T_f}{\partial z^2} \quad (13)$$

Where ρ_f is the density of formation rock, kg/m³; c_f is the specific heat capacity of formation rock, J/(kg·K); λ_{for} is the thermal conductivity of the formation, W/(m·K); ρ_{pf} is the density of pore fluid, kg/m³; c_{pf} is the specific heat capacity of pore fluid, J/(kg·K) and v_r is the pore fluid velocity, m/s.

Using Darcy's law, v_r can be expressed as:

$$v_r = - \frac{\kappa_f}{\mu_{pf} \varphi} \frac{\partial P_p}{\partial r} \quad (14)$$

Where P_p is pore pressure, pa; κ_f is the permeability of formation, D; and μ_{pf} is the viscosity of pore fluid, pa·s.

Substituting Equation (14) into Equation (13) and rearranging yields:

$$\frac{\partial T_f}{\partial t} = \frac{\lambda_{for}}{\rho_f c_f} \left[\left(\frac{\partial^2 T_f}{\partial r^2} + \frac{1}{r} \frac{\partial T_f}{\partial r} \right) + \frac{\partial^2 T_f}{\partial z^2} \right] + \frac{\rho_{pf} c_{pf}}{\rho_f c_f} \frac{\kappa_f}{\mu_{pf} \varphi} \frac{\partial P_p}{\partial r} \frac{\partial T_f}{\partial r} \quad (15)$$

2.3. Auxiliary equation

2.3.1. Calculation of additional heat source term

The heat source terms $q_{p,add}$ and $q_{a,add}$ in equations (6) and (12) for drilling operations include the heat generated by the drilling fluid as it passes through the drill bit, the heat generated by rock fragmentation at the drill bit, and the heat generated by friction between the drill string and the wellbore wall.

As the drilling fluid flows through the nozzle of the drill bit, a substantial pressure drop occurs. This pressure drop subsequently converts into thermal energy, contributing to a heat source term associated with the drill bit pressure drop. The calculation of the heat generated by the conversion of the drill bit pressure drop into thermal energy per unit time can be achieved by employing equation (16):

$$q_{bit,flow} = P_{bit} \cdot Q = \frac{0.081 \rho_p Q^3}{C_d^2 d_{ne}^4} \quad (16)$$

Where P_{bit} is the drill bit pressure drop, MPa; C_d is the flow coefficient of bit nozzles, dimensionless; d_{ne} is equivalent diameter of the bit nozzles, m.

The heat generated by the friction between the drill bit and the formation can be determined by utilizing the general equations proposed by Chang et al. (2018):

$$q_{bit,fri} = \frac{1}{J} (1 - \beta) (WOB * ROP + 2\pi RPM * TOB) \quad (17)$$

Where J is the Joule's constant; β is bit efficiency, dimensionless; WOB is weight on bit, N; ROP is rate of penetration, m/s; RPM is rotational speed, r/min; TOB is torque on bit, N·m.

The heat generated by mechanical friction between drill string and formation/wellbore during rotary drilling process represents a significant heat source for the drilling fluid within the annulus can be determined by applying equations (18) and (19) (Nguyen et al., 2010):

$$q_{drag} = \frac{1}{J} \mu_f w_c 2\pi RPM \quad (18)$$

$$q_{drag} = \frac{1}{J} \mu_f w_c ROP \quad (19)$$

Where μ_f is friction coefficient, dimensionless; w_c is contact force, N.

2.3.2. Determination of heat transfer resistance

The thermal resistances R_{pa} and R_{af} in equations (6) and (12) can be obtained by using Equations (20) and (21).

$$R_{pa} = R_{pai} + R_{pipe} + R_{pao} \quad (20)$$

$$R_{af} = \begin{cases} R_{afi} + R_{cas} + R_{cem} + R_{for} & \text{Cased} \\ R_{afo} + R_{for} & \text{Open hole} \end{cases} \quad (21)$$

Where R_{pai} is the convective heat transfer resistance between the inner wall of drill string and the drilling fluid inside drill string, (K·m)/W; R_{pipe} is the thermal resistance of drill string, (K·m)/W; R_{pao} is the convective

heat transfer resistance between the outer wall of drill string and drilling fluid in annulus, (K·m)/W; R_{afl} is the convective heat transfer resistance between the casing or the wall of the open hole and the drilling fluid in annulus, (K·m)/W; R_{cas} is the thermal resistance of the casing, (K·m)/W; R_{cem} is the thermal resistance of the cement sheath, (K·m)/W; R_{for} is the thermal resistance of the formation, (K·m)/W.

The convective heat transfer resistance per unit length (R_{pao} , R_{pao} , R_{afl}) can be mathematically expressed by equation (22):

$$R_{cov} = \frac{1}{Sh} \quad (22)$$

Where S is the surface area of the heat transfer section, m²; h is the convective heat transfer coefficient, which can be determined through equation (23):

$$h = \frac{Nu\lambda_m}{D_h} \quad (23)$$

Where Nu is Nusselt number; D_h is hydraulic diameter of the flow channel, m; λ_m is the thermal conductivity of the drilling fluid, W/(m·K).

To account for forced convection within the annulus, the convective heat transfer coefficient of the fluid can be adjusted by applying the equivalent Reynolds number proposed by Fénöt et al. (2011), as shown in Equation (24). This correction enables a more accurate estimation of the convective heat transfer coefficient for the annular flow.

$$Nu = 0.023Re_{eff}^{0.8} Pr^{0.5} \quad (24)$$

Where Pr is Prandtl number, Re_{eff} is effective Reynolds number, which can be defined as follows:

$$Re_{eff} = \frac{\rho v_{eff} D_h}{\mu_a} = \left[v_a^2 + \beta \left(\frac{RPM \cdot D_{po}}{2} \right)^2 \right]^{0.5} \frac{\rho_a D_h}{\mu_a} \quad (25)$$

where v_{eff} is the equivalent flow velocity, m/s; μ_a is the annulus fluid apparent viscosity, Pa·s; v_a is the annulus flow velocity, m/s; and β is the equivalent coefficient.

The thermal resistance per unit length (R_{pipe} , R_{cas} , R_{cem}) can be mathematically represented by equation (26):

$$R_{guid} = \frac{1}{2\pi\lambda_s} \ln \left(\frac{D_o}{D_i} \right) \quad (26)$$

Where λ_s is the thermal conductivity of the material, W/(m·K); D_i and D_o is the inner and outer diameters of the specific object, m.

The thermal resistance of the formation (R_{for}) is:

$$R_{for} = \frac{T_D}{2\pi\lambda_{for}} \quad (27)$$

Where T_D is Non-dimensional temperature.

Due to the circulation of drilling fluid, the temperature of surrounding formation undergoes variations. Hence, it becomes essential to incorporate a dimensionless formation thermal time function to elucidate the interplay between thermal resistance and time in this heat transfer phenomenon. In this work, the modified model proposed by Hasan et al. (2010) is employed to, and its representation is provided below:

$$T_D = \ln [e^{-0.2t_D} + (1.5 - 0.3719e^{-t_D})] \sqrt{t_D} \quad (28)$$

$$t_D = \alpha t / r_{wf}^2 \quad (29)$$

Where t_D is dimensionless time; α is thermal diffusivity, m²/s; t is the cumulative contact time of drilling fluid and formation, s; r_{wf} is radius of concentric circle at the wellbore-formation interface, m.

2.3.3. Determination of mud physical parameters

The impact of temperature and pressure conditions on the rheological parameters of drilling fluid is represented by Equations (30)–(32), as presented by:

$$\tau_0 = \tau_{00} \exp [\xi_1(T - T_0) + \xi_2(P - P_0) + \xi_3(T - T_0)^2] \quad (30)$$

$$K = K_0 \exp [\xi_4(T - T_0) + \xi_5(P - P_0) + \xi_6(T - T_0)^2] \quad (31)$$

$$n = n_0 \exp [\xi_7(T - T_0) + \xi_8(P - P_0) + \xi_9(T - T_0)^2] \quad (32)$$

Where τ_{00} is yield point of the drilling fluid at the reference temperature and pressure, Pa; K_0 is consistency coefficient of the drilling fluid at the reference temperature and pressure, Pa·sⁿ; n_0 is flow behavior index of the drilling fluid at the reference temperature and pressure; ξ_1 to ξ_9 are characteristic parameters of the drilling fluid and are required to be determined through experimental data analysis. This paper employs laboratory data, from which the following coefficients were fitted: $\xi_1 = -0.0095$, $\xi_2 = 3.8132 \times 10^{-9}$, $\xi_3 = 1.0011 \times 10^{-6}$, $\xi_4 = -0.0095$, $\xi_5 = 2.7561 \times 10^{-9}$, $\xi_6 = 1.3751 \times 10^{-6}$, $\xi_7 = -0.0095$, $\xi_8 = 3.8132 \times 10^{-9}$, $\xi_9 = 1.5735 \times 10^{-6}$.

Empirical equations were proposed by Zheng et al. (2018) to describe the correlation between thermal conductivity and specific heat of water in relation to temperature. These equations can be further extended and utilized to characterize drilling fluid parameters:

$$\lambda_f = a_1 + a_2 T + a_3 T^{1.5} + a_4 T^2 + a_5 T^{0.5} \quad (33)$$

$$c_f = b_1 + b_2 T + b_3 T^{1.5} + b_4 T^2 + b_5 T^{0.5} \quad (34)$$

Where λ_f is the thermal conductivity of the drilling fluid, W/(m·K); c_f is the specific heat capacity of the drilling fluid, J/(kg·K); $a_1, a_2, a_3, a_4, a_5, b_1, b_2, b_3, b_4, b_5$ are empirical constants that require determination through experimental data analysis. Specifically, the values assigned to these coefficients are as follows: $a_1 = 0.8456$, $a_2 = 0.0155$, $a_3 = -0.0015$, $a_4 = 5.66 \times 10^{-5}$, $a_5 = -0.0649$, $b_1 = 1583.133$, $b_2 = -7.2036$, $b_3 = 2.9399$, $b_4 = -0.3633$, $b_5 = 0.0146$.

2.4. Boundary conditions

The boundary conditions of the model can be defined as follows:

(1) At the surface, the temperature of the drilling fluid entering the drill pipe remains constant throughout the drilling process and Annular outlet pressure is a fixed value, denoted as follows:

$$T_{p,0}^0 = T_{p,0}^1 = T_{p,0}^2 = \dots = T_{p,0}^n = T_{p,0} \quad (35)$$

$$P_{a,0}^0 = P_{a,0}^1 = P_{a,0}^2 = \dots = P_{a,0}^n = P_{a,0} \quad (36)$$

(2) At bottom hole, the drilling fluid is immediately redirected to the annulus after being discharged through the drill pipe. Consequently, the temperature and pressure of the drilling fluid within the drill pipe is identical to that within the annulus, referred to as:

$$T_{p,max}^0 = T_{a,max}^0, T_{p,max}^1 = T_{a,max}^1, T_{p,max}^2 = T_{a,max}^2, T_{p,max}^n = T_{a,max}^n \quad (37)$$

$$P_{p,max}^0 = P_{a,max}^0, P_{p,max}^1 = P_{a,max}^1, P_{p,max}^2 = P_{a,max}^2, P_{p,max}^n = P_{a,max}^n \quad (38)$$

(3) For surrounding formation, the formation temperature at an infinite distance from the wellbore remains constant and can be characterized by a simple geothermal gradient relationship.

$$T_{f,i}^0 = T_{f,i}^1 = T_{f,i}^2 = \dots = T_{f,i}^n = T_{f,0}^n + g_f \cdot TVD \quad (39)$$

2.5. Initial conditions

The initial formation temperature is adopted as the initial wellbore temperature for simulation, the static hydraulic pressure can serve as the

initial wellbore pressure.

$$T_{p,i}^0 = T_{a,i}^0 = T_{f,i}^0 \quad (40)$$

$$P_{a,i}^0 = \rho_a \cdot g \cdot TVD_i + \sum \Delta P_{a,i} \cdot \Delta L \quad (41)$$

$$P_{p,i}^0 = \rho_p \cdot g \cdot TVD_i + \sum \Delta P_{p,i} \cdot \Delta L + P_{a,max}^0 + P_{bit} \quad (42)$$

Where $\Delta P_{a,i}$ and $\Delta P_{p,i}$ represent the annular pressure loss gradient and the pipe pressure loss gradient at node i, respectively, expressed in MPa/m. The calculation methods can be determined with reference to the provided literature (Mitchell and Miska, 2011).

2.6. Solution

The wellbore formation transient heat transfer model discussed earlier involves a set of partial differential equations. To solve this numerical model, the full implicit finite difference method can be employed. The specific model solving method and solution process can be referred to in Appendix 1.

3. Results and discussions

3.1. Case discussion

Utilizing fundamental data from the Utah FORGE geothermal field, a simulation analysis was conducted to assess the impact of various factors on the temperature distribution of drilling fluid (Utah FORGE Data, 2022). In this specific scenario, the kick-off depth is approximately 600 m, with the inclination angle reaching 90° at around 3800 m and continuing steadily thereafter. The azimuth angle remains constant at 112.35°. The well geometry structure was assumed to be similar to the typical FORGE well configuration outlined in Table 2, with the default conditions used as a reference.

3.2. Circulation time

Utilizing the parameters delineated in Tables 1 and 2, this study conducts simulations to elucidate the impact of individual parameters on the temperature distribution. It is postulated that the initial borehole temperature is equivalent to the original formation temperature, and the subsurface properties are assumed to be isotropic. The inlet temperature of the drilling fluid is specified at 40 °C, and the pumping flow rate is maintained at a constant value of 32.6 L/s. Leveraging the thermal model established in preceding sections, the dynamic temporal variations in temperature within the drill string, annulus, and proximal formation near the borehole wall are discerned.

Table 1

Summary of simulation inputs for base case scenario, inspired from FORGE dataset.

Geometry	
Hole size (m)	0.22
Well depth (m)	2657
Fluid Properties	
Fluid type	Water-based mud
Density (kg/m³)	1067
Fluid plastic viscosity (mPa·s)	14
Specific heat capacity (J/(kg·K))	3750
Thermal conductivity (W/(m·K))	0.75
Formation and Geothermal Properties	
Formation surface temperature (°C)	38
Formation gradient (°C/km)	70
Rock density (kg/m³)	2800
Specific heat capacity (J/(kg·K))	930
Thermal conductivity (W/(m·K))	2.31

Table 2
well geometry structure.

	Inner Diameter (m)	Outer Diameter (m)	MD(m)	Thermal Conductivity (W/(m·K))
Conductor casing	0.48	0.51	39	45
Surface casing	0.32	0.34	116	45
Intermediate casing	0.22	0.24	1063	45
Open hole	–	0.22	528–1055	45
DP	0.11	0.127	2290	45
HWDP	0.083	0.127	223	45
DC	0.073	0.17	143	45
Drill bit	–	0.22	0.8	45

Fig. 3 simulates the temporal evolution of drilling fluid temperatures within the wellbore and the adjacent formation at a depth of 6800 m (with a horizontal section length of approximately 3000 m) over a 20-h circulation process. As depicted in Fig. 3, in the upper section of the wellbore, with increasing circulation time at the same well depth, the drilling fluid temperature rises and surpasses the original formation temperature. Conversely, in the lower section of the wellbore, the drilling fluid temperature decreases with increasing circulation time, falling below the original formation temperature. This observed phenomenon is attributed to the continuous transfer of heat from the lower formation to the upper formation through convective and conductive heat exchange in the annular fluid. Consequently, as circulation time increases, the lower formation gradually cools, leading to a reduction in the lower formation temperature, while the drilling fluid temperature in the wellbore decreases. Conversely, the upper formation experiences a gradual heating, resulting in an increase in the upper formation temperature.

In order to further comprehend the temporal variations of wellbore temperature during the circulation process, Fig. 4 simulates the evolution of DHT and wellhead temperature over a continuous 50-h circulation period. As depicted in Fig. 3, during the initial stages of circulation (<5 h), both the wellhead and DHT exhibit significant fluctuations, with the DHT rapidly decreasing from 208.554 °C to 107.411 °C after 50 h of circulation, representing a reduction of approximately 48.5%. The decreasing rate of temperature change for both the wellhead and DHT diminishes as circulation time progresses. This phenomenon can be attributed to the substantial temperature differential between the wellbore and formation at the onset of circulation, resulting in high thermal exchange efficiency and rapid temperature variations. As circulation time increases, the wellbore temperature and formation temperature gradually approach equilibrium, leading to a diminished temperature differential and reduced thermal exchange efficiency. Consequently, the rate of temperature change gradually decreases.

3.3. Length of horizontal

Based on the wellbore trajectory design, the well reaches a deviation angle of 90° at a depth of 3800 m, after which horizontal drilling commences. Fig. 5 illustrates the DHT distribution curves corresponding to different horizontal section lengths during a 20-h circulation process. As depicted in Fig. 5, for well depths of 3800 m (with an approximate horizontal section length of 0 m), 4200 m (with an approximate horizontal section length of 400 m), 4800 m (with an approximate horizontal section length of 1000 m), 5200 m (with an approximate horizontal section length of 1400 m), 6000 m (with an approximate horizontal section length of 2200 m), and 7000 m (with an approximate horizontal section length of 3200 m), the calculated DHT at the points when the temperatures essentially stabilize are 89.7 °C, 100.08 °C, 114.718 °C, 123.92 °C, 139.897 °C and 156.291 °C, respectively.

Fig. 6 summarizes the influence of horizontal section lengths on DHT, revealing a gradual convergence of DHT towards the formation

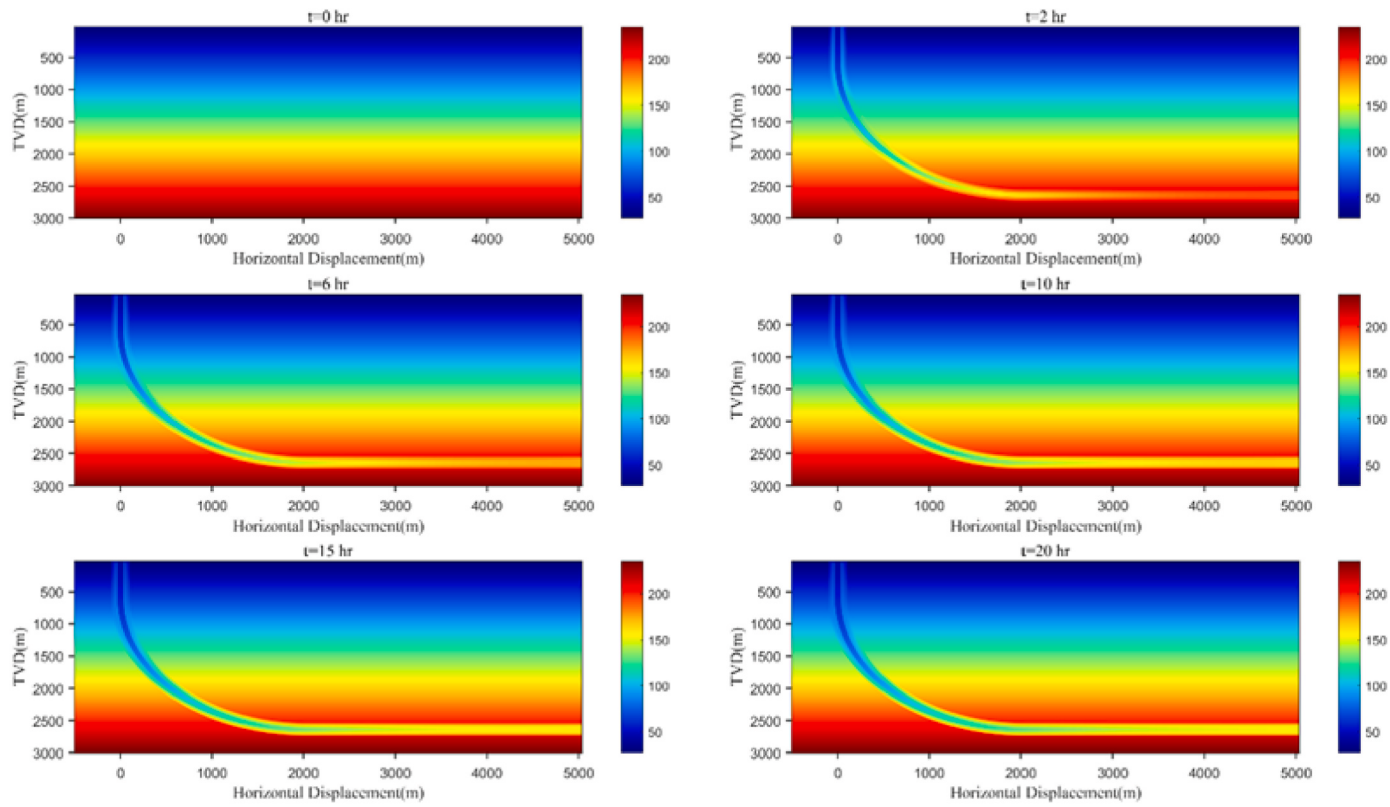


Fig. 3. The temperature distribution within the wellbore and formation at different circulation times.

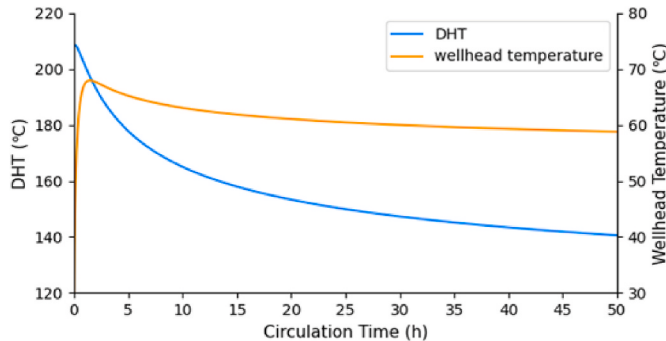


Fig. 4. DHT and wellhead temperature distribution under circulation time.

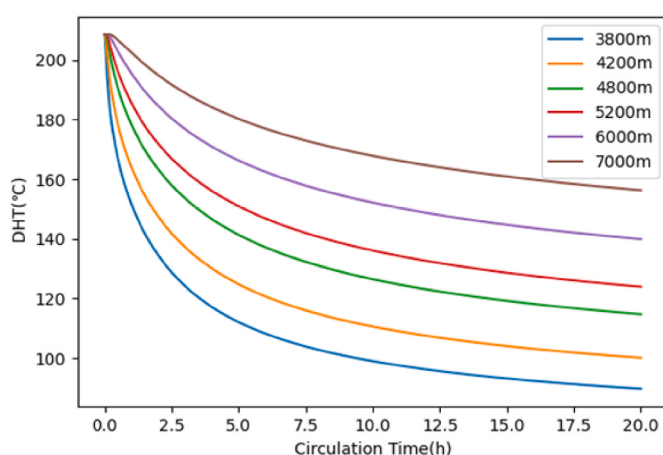


Fig. 5. The distribution of DHT at varying well depths.

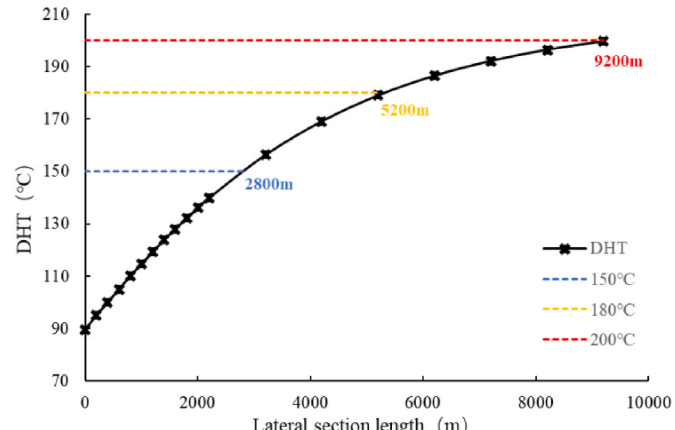


Fig. 6. Steady DHT VS horizontal section length.

temperature with increasing horizontal section length. At the same vertical depth, a longer horizontal section corresponds to a higher temperature within the respective horizontal section. The extension of the horizontal section noticeably amplifies the DHT; however, this rate of increase diminishes progressively with the augmentation of the horizontal section length. This phenomenon arises from the extended length of the horizontal section, resulting in a more prolonged flow of drilling fluid within the stable high-temperature environment of the horizontal wellbore. Consequently, the longer exposure time enhances the thermal exchange with the surrounding formation, leading to greater heat absorption and, subsequently, higher temperatures.

3.4. Flow rate

Fig. 7 depicts the influence of drilling fluid circulation rates on the

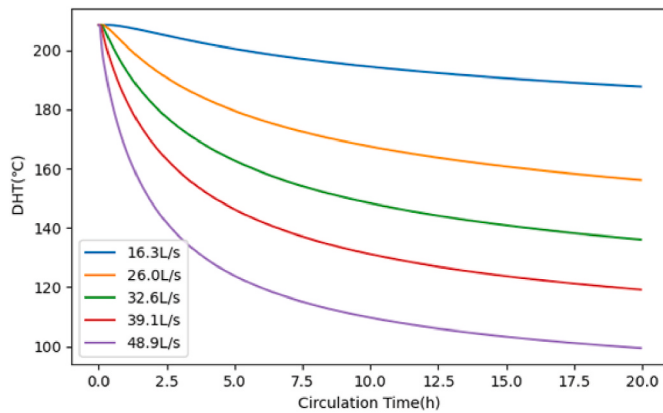


Fig. 7. The distribution of DHT at varying flow rate.

distribution of DHT. As delineated in the figure, circulation rates of 16.3 L/s (equivalent to an annular return velocity of approximately 0.5 m/s), 26 L/s (annular return velocity approximately 0.8 m/s), 32.6 L/s (annular return velocity approximately 1.0 m/s), 39.1 L/s (annular return velocity approximately 1.2 m/s), and 48.9 L/s (annular return velocity approximately 1.5 m/s) result in calculated stable DHT of 187.737 °C, 156.233 °C, 136.106 °C, 119.19 °C, and 99.452 °C, respectively. For a constant horizontal section length, an augmentation in circulation flow rate significantly attenuates the distribution of DHT. This phenomenon is attributed to the increased circulation rates, which, for a fixed distance of horizontal section length, curtail the circulation contact time of drilling fluid within the wellbore.

However, in the context of an extended horizontal section, the augmentation of horizontal section length during the circulation process results in a prolonged contact time between the drilling fluid and the formation. Consequently, the drilling fluid absorbs a substantial amount of heat from the formation, as depicted in Fig. 8.

3.5. Inlet temperature

Fig. 9 illustrates the impact of drilling fluid inlet temperature on the distribution of DHT. The DHT decreases with a reduction in the drilling fluid inlet temperature, wherein a decrease of 10 °C in the inlet temperature correlates with an approximately 2.9 °C decrease in the DHT. Although the magnitude of reduction is modest, the utilization of lower temperature drilling fluids as a means of absorbing heat from the formation is considered feasible, particularly in cases where the horizontal section length is relatively small.

Fig. 10 illustrates the impact of inlet temperature on the distribution of DHT under various horizontal section lengths. As depicted in Fig. 9, a decrease in drilling fluid inlet temperature induces cooling effects on the DHT during the circulation process, primarily influencing the fluid temperature in short horizontal well sections. However, with the extension of the horizontal well section, the increased circulation contact time, coupled with the sustained influence of the formation's high

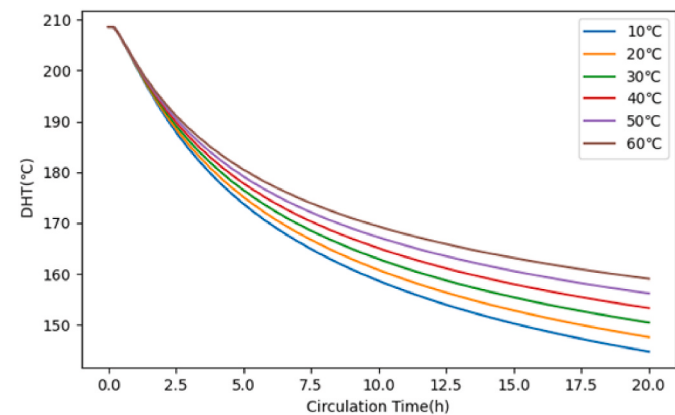


Fig. 9. The distribution of DHT at varying inlet temperature.

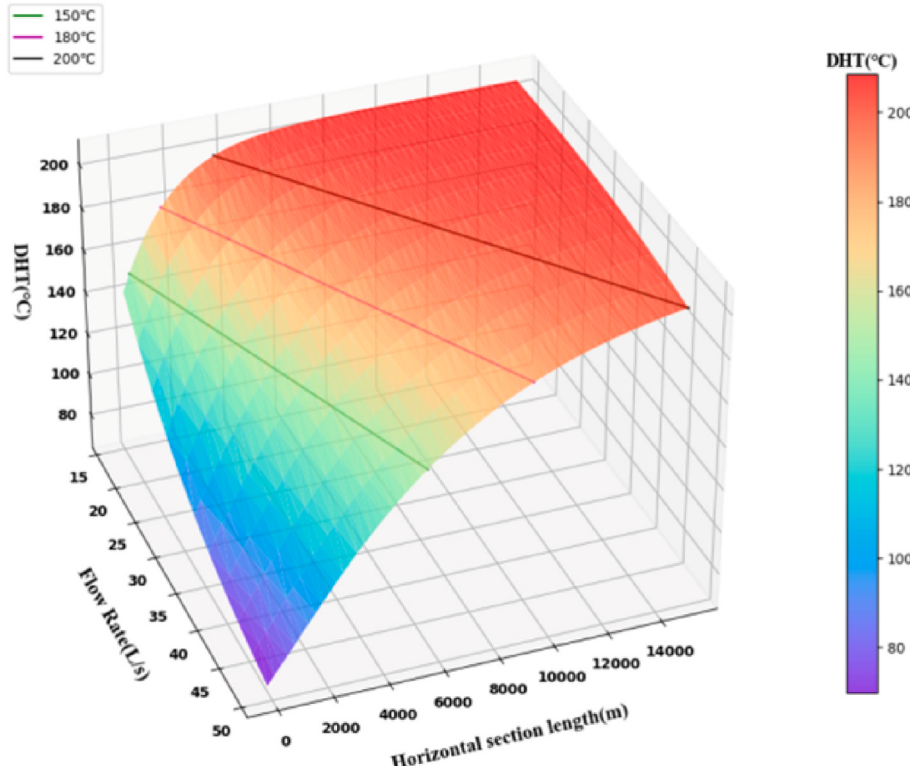


Fig. 8. Impact of flow rate on the DHT with different horizontal section length.

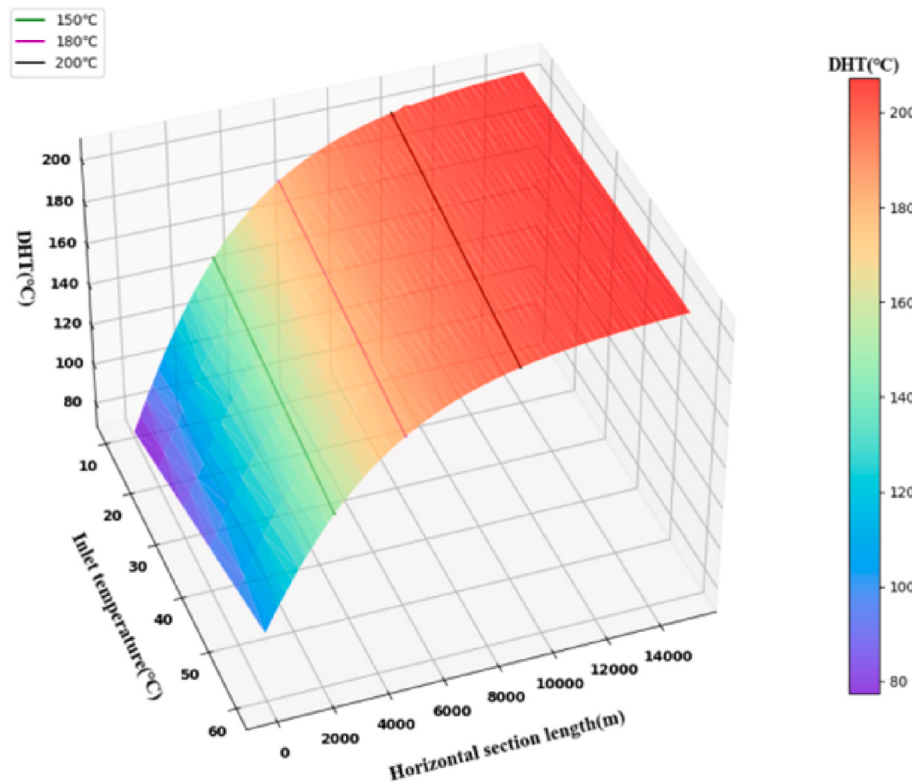


Fig. 10. Impact of inlet temperature on the DHT with different horizontal section length.

temperature, leads to a significant impact of the formation temperature on the circulation temperature field. Consequently, this diminishes the influence of the inlet temperature.

3.6. Fluid density

The DHT influenced by drilling fluid density is depicted in Fig. 11, wherein the DHT decreases from 153.3 °C to 88.867 °C for drilling fluid densities ranging from 1067 kg/m³ to 2267 kg/m³. This observation indicates that under identical circulation conditions, the DHT gradually decreases with an increase in fluid density. The rationale behind this phenomenon lies in the higher density of the drilling fluid, leading to a greater mass per unit volume. Consequently, more heat is absorbed during the thermal exchange process, resulting in a rapid decrease in the surrounding formation temperature. Simultaneously, as drilling fluid density increases, the rate of decrease in DHT gradually diminishes.

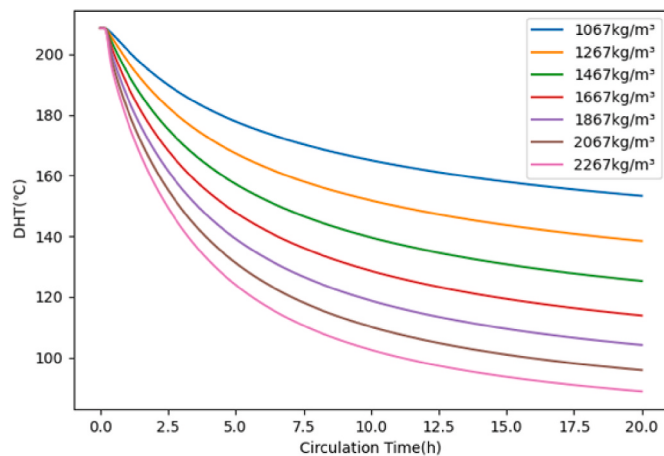


Fig. 11. The distribution of DHT at varying fluid density.

3.7. Fluid heat capacity

Fig. 12 illustrates the impact of fluid heat capacity on the DHT, showcasing a decrease in DHT with an increase in fluid heat capacity. As depicted in Fig. 12, with fluid heat capacity ranging from 1000 J/(kg·K) to 4000 J/(kg·K), the DHT undergoes a variation from 207.09 °C to 147.836 °C after 20 h of circulation. This phenomenon arises due to the higher heat capacity of the fluid under specific temperature differentials during heat exchange, resulting in the transfer of more heat from the bottomhole to the surface and consequent reduction in DHT.

3.8. Formation thermal conductivity

The thermal conductivity of the formation fundamentally governs the efficiency of heat conduction within the subsurface. Fig. 13 delineates the correlation between DHT and the thermal conductivity of the formation. As the thermal conductivity of the formation ascends, the

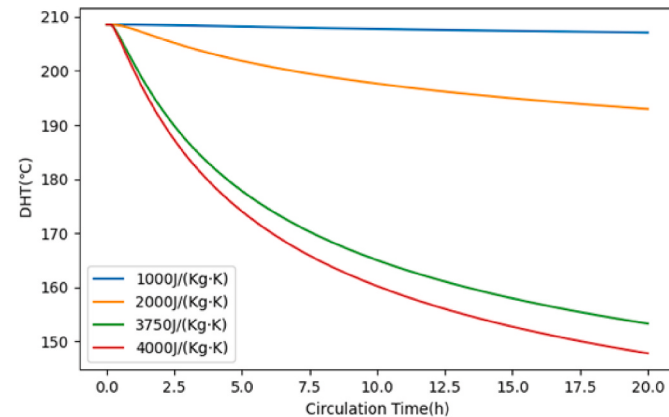


Fig. 12. The distribution of DHT at varying fluid heat capacity.

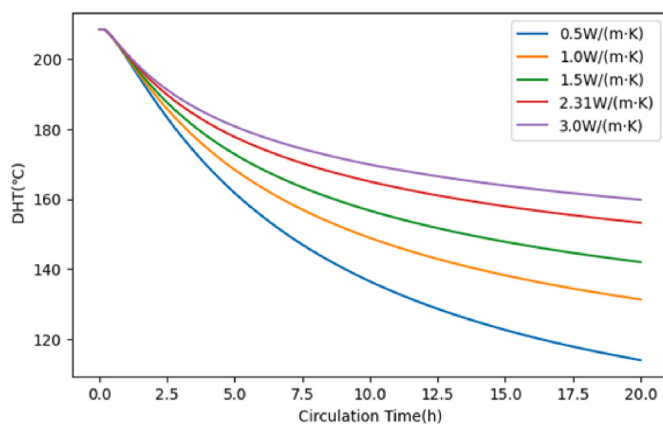


Fig. 13. The distribution of DHT at varying formation thermal conductivity.

DHT concurrently rises, signifying that an augmented thermal conductivity in the formation results in a greater transfer of heat to the annular space. As depicted in Fig. 13, with the thermal conductivity of the formation escalating from $0.5 \text{ W}/(\text{m}\cdot\text{K})$ to $3.0 \text{ W}/(\text{m}\cdot\text{K})$, the DHT undergoes a transition from 114.052°C to 159.85°C after 20 h of circulation.

3.9. Drill pipe thermal conductivity

The impact of drill pipe thermal conductivity on DHT is depicted in Fig. 14, with thermal conductivities of $45 \text{ W}/(\text{m}\cdot\text{K})$ and $3.12 \text{ W}/(\text{m}\cdot\text{K})$ representing standard carbon steel drill pipes and Insulated Drill Pipes (IDPs), respectively, while other values correspond to various thermal conductivity settings defined in the simulation. Variations in drill pipe thermal conductivity exert a notable influence on the temperature of the annular drilling fluid, with the IDP, characterized by a lower thermal conductivity, demonstrating a more rapid reduction in DHT.

Fig. 14 further illustrates that when the thermal conductivity of the drill pipe experiences a minor decrease, the impact on DHT is negligible. However, a significant reduction in the drill pipe's thermal conductivity leads to a substantial decrease in DHT. As depicted in the figure, when the drill pipe's thermal conductivity is $45 \text{ W}/(\text{m}\cdot\text{K})$, the DHT is 153.3°C . As it decreases to $30 \text{ W}/(\text{m}\cdot\text{K})$ and $20 \text{ W}/(\text{m}\cdot\text{K})$, the DHT only decreases by approximately 3.1%, with a modest cooling rate. However, when the cooling rate drops to $5 \text{ W}/(\text{m}\cdot\text{K})$, the DHT significantly decreases to 128.292°C . These findings underscore the efficacy of insulated drill pipes as a superior geothermal well drilling method, effectively reducing DHT.

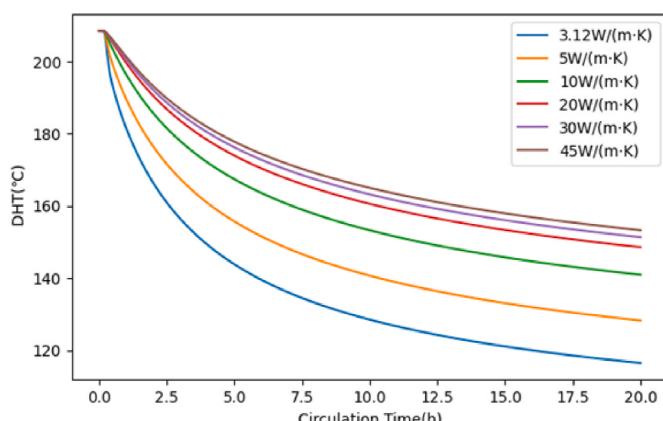


Fig. 14. The distribution of DHT at varying Drill pipe thermal conductivity.

4. Sensitivity analysis

The foregoing analysis has identified potential input parameters that may influence wellbore temperature. In practical applications, due to the stochastic nature of operational parameters, a variety of different combinations may exist, resulting in diverse computational outcomes. When numerous factors are involved, the number of generated scenarios becomes immense, rendering it impractical to simulate wellbore temperature distributions by altering various scenarios. To accurately assess the impact of each parameter, it is imperative to integrate sensitivity analysis techniques with Monte Carlo sampling methods. This combination allows for the simulation of the influence of each parameter on wellbore temperature distribution, thereby determining the most significant factors affecting wellbore temperature distribution. This approach provides a more scientifically grounded basis for decision-making in the development and temperature control of geothermal wells. The steps involved in conducting data simulation using Monte Carlo method generally include: (1) Determination of input parameter ranges: Establishing the possible value ranges for each input parameter used in the simulation, including minimum, maximum, and most likely values; (2) Selection of probability distributions: Choosing appropriate probability distributions for each input parameter, commonly used distributions include triangular distribution, uniform distribution, normal distribution, etc.; (3) Generation of random samples: Employing the Monte Carlo method to generate a large number of random samples based on the selected probability distributions, representing the potential values of each input parameter; (4) Simulation computation: Performing calculations using the model for each random sample to obtain corresponding output results; (5) Result analysis: Gathering all simulation results and conducting statistical analysis, such as probability distribution and probability density functions.

The input parameters utilized in this study are assumption-based, yet the range of variations for each input parameter needs to be rational and consistent with the represented real-world data. From an engineering perspective, triangular and uniform distributions are preferred for wellbore temperature calculations (Williamson et al., 2006). For the aforementioned real-world data case, this paper adopts a triangular distribution as the probability distribution criterion for assumed input parameters. For the analysis of the specific parameter impact, the maximum value (a), minimum value (b), and most likely value (c) for each input parameter are considered. A total of 5000 random samples for each impacting parameter are generated to establish the corresponding triangular distribution. The probability distribution and probability density of the discharge after 5000 Monte Carlo experiments are presented in Fig. 14, where a, b, and c correspond to discharge values of 16.3, 48.9, and 32.6 L/s, respectively. The P10, P50, and P90 probability values for flow rate represent low probability, medium probability, and high probability, as illustrated by the purple, yellow, and red dashed lines in Fig. 15, corresponding to 19.56, 32.6, and 45.64 L/s, respectively. Similar processing procedures are applied for other impacting parameters, and the low, medium, and high probability values for each sensitive parameter are summarized in Table 3.

Parameter sensitivity analysis involves assessing the extent of the influence of each input parameter on the final wellbore temperature distribution under existing potential combinations of input parameters. This necessitates the quantification of the contribution of each parameter to the variation in DHT through the utilization of Monte Carlo methods and a heat transfer model. While employing Monte Carlo methods to obtain the probability distribution of each input parameter, the integration of the heat transfer model solver enables the determination of the impact of input parameters on the probability density and cumulative probability of the DHT distribution. As demonstrated in Fig. 16, which illustrates the influence on discharge, the P90, P50, and P10 values are 173.21°C , 150.37°C , and 126.42°C , respectively. This signifies that the probability of the DHT being $\leq 173.21^\circ\text{C}$ is 90%, $\leq 150.37^\circ\text{C}$ is 50%, and $\leq 126.42^\circ\text{C}$ is 10%.

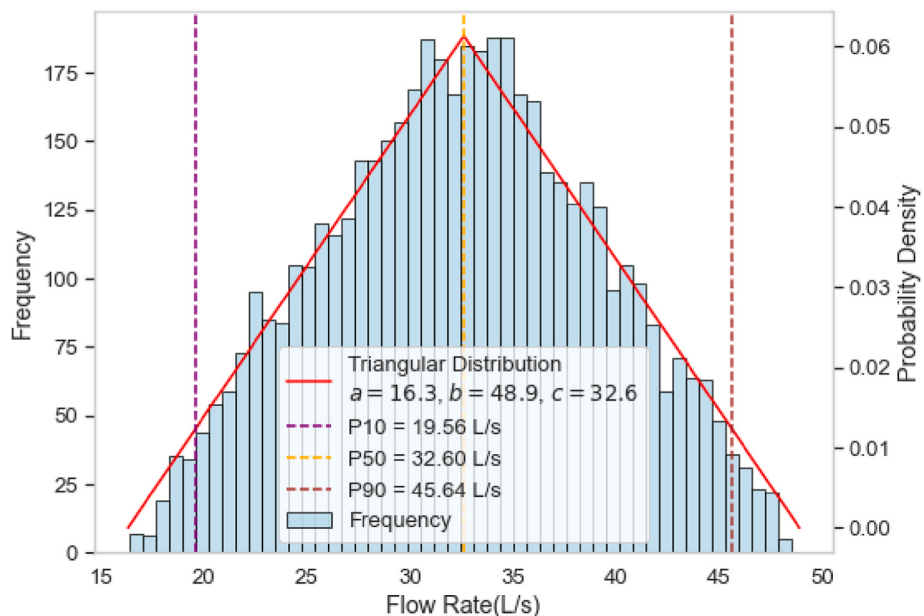


Fig. 15. Flow rate probability distribution.

3

Data analysis for each sensitive parameter from triangular distribution.

Sensitivity parameter	P10	P50	P90	Unit
Circulation time	2	10	18	h
Flow rate	19.56	32.6	45.64	L/s
Horizontal section length	1000	3000	9000	m
Inlet temperature	10	35	55	°C
Fluid density	650	1250	1850	Kg/m³
Fluid heat capacity	1100	2500	3900	J/(Kg·K)
Formation thermal conductivity	1.06	3.70	6.34	W/(m·K)
Drill pipe thermal conductivity	4.58	22.55	40.51	W/(m·K)
DHT		184.80		°C

In the context of sensitivity analysis, the One-at-a-time (OAT) method is employed to quantify the individual contribution of each input parameter to the DHT. Specifically, the OAT method designates the evaluated input parameters as random variables, while treating all other input parameters as fixed inputs with P50 values. This method involves incrementally varying a specific input parameter in each iteration to examine the impact of this variation on the output results. Notably, all input parameters utilize the calibrated values calculated

based on the P50, as DHT indicated in Table 3.

Utilizing the aforementioned methodology, similar simulations were conducted to assess the extent of influence of each input parameter on the DHT. Based on the simulation outcomes, the impact of input parameters was ranked, and the results were elucidated through a sensitivity tornado chart, as illustrated in Fig. 17.

In the context where other parameters remain constant, the length of the horizontal section and the circulation rate directly influence the circulation time of the drilling fluid in the wellbore, with the length of the horizontal section playing a significant role in the DHT (44.17%). Additionally, the properties of the drilling fluid, including thermal capacity and density, also have a substantial impact on the DHT, accounting for 40.79% and 35.11%, respectively. Although the thermal conductivity of the formation and drill string depends on material properties, components such as near-surface casing, cement sheath, and insulated drill pipes can alter the thermal conductivity around the drilling fluid. Using materials with lower thermal conductivity proves effective in controlling wellbore temperature when feasible. Compared to other input parameters, the influence of circulation time and injection temperature on the temperature control of geothermal horizontal wells is relatively modest. The analysis results indicate that attention should

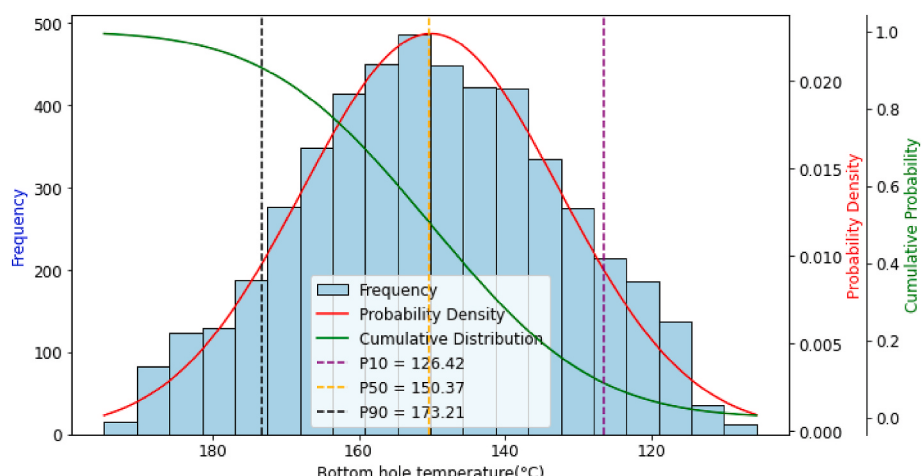


Fig. 16. The relationship between the probability distribution and bottom-hole temperature.

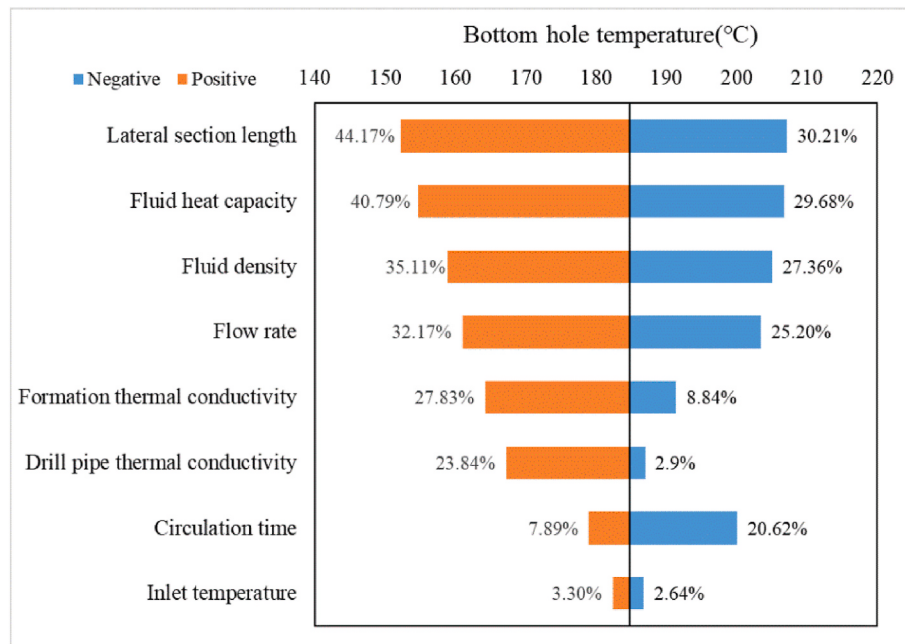


Fig. 17. Sensitivity tornado chart.

be focused on the design of the horizontal section length, selection of drilling fluid and pipe, and circulation rate to achieve effective control of wellbore temperature. However, given that the drilling process is a highly complex and coupled system, temperature control efforts need to consider the impact of these parameter changes on other outcomes of the drilling process, such as pressure and cuttings distribution. Additionally, the sensitivity depicted in Fig. 17 may vary depending on the specific application context, necessitating a new analysis using the same methodology tailored to the desired application.

5. Geothermal well drilling workflow

The entire workflow for geothermal well temperature control is illustrated in Fig. 18. As depicted in the figure, input parameters are categorized into two types based on their correlation with on-site conditions. The first category comprises controllable parameters such as pumping flow rate, injection temperature, and fluid properties. The second category includes uncontrollable parameters, given the limited options for materials such as drill pipes and casings due to their fixed nature. In practical applications, an assessment of whether parameters

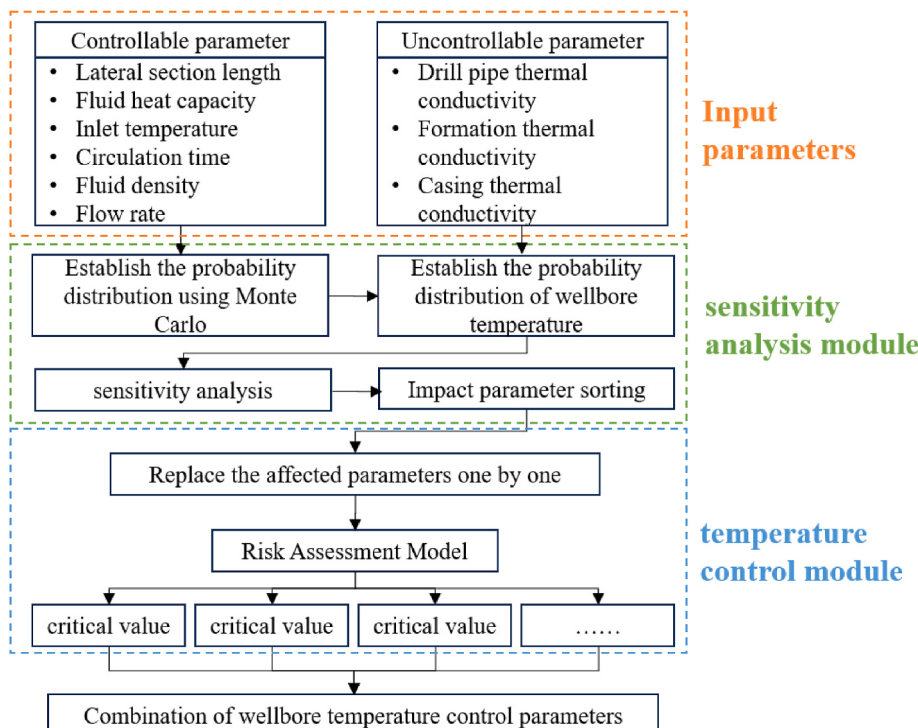


Fig. 18. Workflow for wellbore temperature management in geothermal wells.

can be altered based on on-site conditions can be conducted to identify controllable input parameters. The workflow is outlined as follows.

- Performing a statistical analysis on the reasonable distribution ranges of all controllable input parameters, the Monte Carlo method is employed to obtain the probability distribution of input values.
- For each simulated combination of input values, the calculation of temperature distribution along the wellbore and the near-wellbore formation is conducted. Subsequently, a probability distribution for the DHT is established.
- Upon completing all simulated combinations, a sensitivity analysis is conducted to ascertain the contribution levels of all controllable input parameters to the wellbore temperature. Subsequently, these contributions are ranked based on their respective importance.
- The sorted influential parameters, ranging from high to low impact, are sequentially substituted into the risk assessment model (the specific model used for evaluation is provided separately to determine if the current parameter combination might induce subsurface risks). This process aims to identify the critical thresholds at which each input parameter positively contributes to reducing DHT.
- Upon identifying the critical thresholds for all input parameters, the final step involves gathering these critical values to guide the configuration of control parameters for wellbore temperature.

6. Conclusions

This study introduces a quantitative method to assess the relative importance of various parameters in influencing the temperature distribution within a geothermal horizontal well, aiming to achieve efficient management of wellbore temperatures. By combining a transient heat transfer model and sensitivity analysis, the impact of input parameters on DHT is evaluated, leading to the establishment of an effective wellbore temperature management process. The key findings are as follows:

The transient heat transfer model developed in this study takes into account various factors, including wellbore structure, multiple heat sources, and variations in drilling fluid properties with temperature and pressure. It proves applicable for the assessment and management of wellbore temperatures in geothermal horizontal wells with long horizontal sections.

A detailed analysis of the impact of each parameter on wellbore temperature is conducted. The results indicate that DHT increases with longer horizontal section lengths, higher entry temperatures, greater formation thermal conductivity, and increased drilling rod thermal conductivity. Conversely, it decreases with higher drilling fluid heat capacity, lower drilling fluid density, larger circulation rates, and extended circulation times.

Utilizing Monte Carlo methods, the study calculates and analyzes the

relative importance of each input parameter in influencing the DHT distribution in geothermal horizontal wells. The order of importance is identified as follows: horizontal section length > drilling fluid heat capacity > drilling fluid density > circulation rate > formation thermal conductivity > drilling rod thermal conductivity > circulation time > entry temperature.

A workflow tailored for practical geothermal drilling design is formulated, providing a comprehensible guide for field engineers and offering valuable insights for drilling design and operations.

The limitations of this study lie in the narrow focus on analyzing the importance ranking of temperature management and the maximum length of horizontal sections solely from the perspective of temperature restrictions, while disregarding other factors influencing horizontal section length, such as hydraulic limitations, mechanical constraints, geological factors, and economic considerations. Future research directions may involve integrating these various constraints to establish more rigorous criteria for decision-making, thereby achieving optimization of solutions from a holistic perspective.

CRediT authorship contribution statement

Xi Wang: Writing – original draft, Software, Methodology, Formal analysis. **Feifei Zhang:** Writing – review & editing, Supervision, Resources, Methodology, Investigation, Funding acquisition, Conceptualization. **Xueying Wang:** Project administration, Formal analysis, Data curation. **Yibin Yu:** Validation, Investigation. **Wenqiang Lou:** Investigation, Data curation. **Fengjia Peng:** Visualization, Validation.

Declaration of competing interest

The authors declare the following financial interests/personal relationships which may be considered as potential competing interests:

Feifei Zhang reports financial support was provided by National Natural Science Foundation of China. Feifei Zhang reports financial support was provided by Hubei Provincial Science and Technology Agency. If there are other authors, they declare that they have no known competing financial interests or personal relationships that could have appeared to influence the work reported in this paper.

Data availability

Data will be made available on request.

Acknowledgements

This work was supported by Department of Science and Technology of Hubei Province [2023BCB111]; and Department of Education of Hubei Province [NO.T2021004].

Appendix 1. Model Solution

In this paper, the fully implicit finite difference method is adopted to solve the model discussed earlier. Firstly, the entire wellbore and the surrounding formation near the wellbore are discretized into grids, as shown in Fig. 19. Then, the model is discretized in both time and space, transforming the mathematical model into a finite difference form, as shown in Equations (1-1) and (1-2). By solving the resulting equations, the numerical solution of the wellbore temperature field is obtained.

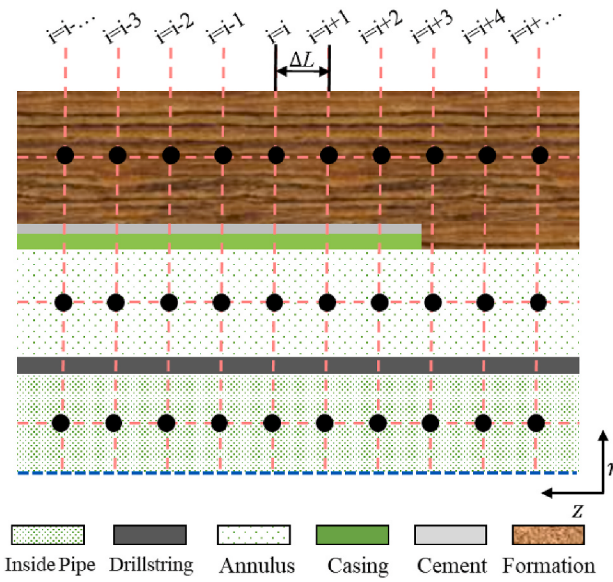


Fig. 19 Diagram of the mesh grids of the wellbore and formation.

According to the fully implicit finite difference method, equations (6) and (12) can be respectively transformed into:

$$\frac{\pi D_{pi}^2}{4} \frac{(c\rho)_{p,i}^{n+1} T_{p,i}^{n+1} - (c\rho)_{p,i}^n T_{p,i}^n}{\Delta t} = \frac{T_{a,i}^{n+1} - T_{p,i}^{n+1}}{R_{pa}} + \rho_p Q \frac{c_{p,i}^{n+1} T_{p,i}^{n+1} - c_{p,i-1}^{n+1} T_{p,i-1}^{n+1}}{\Delta z} + q_{p,add}^{n+1} \quad (1-1)$$

$$\left[\frac{\pi(D_{ai}^2 - D_{po}^2)}{4} \frac{(c\rho)_{a,i}^{n+1}}{\Delta t} + \frac{1}{R_{pa}} + \frac{1}{R_{af}} - \frac{\rho_p Q c_{a,i}^{n+1}}{\Delta z} \right] T_{a,i}^{n+1} - \frac{\pi(D_{ai}^2 - D_{po}^2)}{4} \frac{(c\rho)_{a,i}^n T_{a,i}^n}{\Delta t} - \frac{1}{R_{pa}} T_{p,i}^{n+1} + \frac{\rho_p Q c_{a,i-1}^{n+1}}{\Delta z} T_{a,i-1}^{n+1} = q_{a,add}^{n+1} + \frac{T_{f,i}^{n+1}}{R_{af}} \quad (1-2)$$

By consolidating like terms, the discretized equation can be obtained as:

$$a_{p,i}^{n+1} T_{p,i}^{n+1} + a_{p,i}^n T_{p,i}^n + a_{a,i}^{n+1} T_{a,i}^{n+1} + a_{p,i-1}^{n+1} T_{p,i-1}^{n+1} = a_{p,add}^{n+1} \quad (1-3)$$

$$b_{a,i}^{n+1} T_{a,i}^{n+1} + b_{a,i}^n T_{a,i}^n + b_{p,i}^{n+1} T_{p,i}^{n+1} + b_{a,i-1}^{n+1} T_{a,i-1}^{n+1} = b_{p,add}^{n+1} \quad (1-4)$$

Where:

$$a_{p,i}^{n+1} = \frac{\pi D_{pi}^2 (c\rho)_{p,i}^{n+1}}{\Delta t} + \frac{1}{R_{pa}} - \frac{\rho_p Q c_{p,i}^{n+1}}{\Delta z} \quad (1-5)$$

$$a_{p,i}^n = -\frac{\pi D_{pi}^2 (c\rho)_{p,i}^n}{\Delta t} \quad (1-6)$$

$$a_{a,i}^{n+1} = -\frac{1}{R_{pa}} \quad (1-7)$$

$$a_{p,i-1}^{n+1} = \frac{\rho_p Q c_{p,i-1}^{n+1}}{\Delta z} \quad (1-8)$$

$$a_{p,add}^{n+1} = q_{p,add}^{n+1} \quad (1-9)$$

$$b_{a,i}^{n+1} = \frac{\pi(D_{ai}^2 - D_{po}^2)}{4} (c\rho)_{a,i}^{n+1} + \frac{1}{R_{pa}} + \frac{1}{R_{af}} - \frac{\rho_p Q c_{a,i}^{n+1}}{\Delta z} \quad (1-10)$$

$$b_{a,i}^n = -\frac{\pi(D_{ai}^2 - D_{po}^2)}{4} (c\rho)_{a,i}^n T_{a,i}^n \quad (1-11)$$

$$b_{p,i}^{n+1} = -\frac{1}{R_{pa}} \quad (1-12)$$

$$b_{a,i-1}^{n+1} = \frac{\rho_p Q c_{a,i-1}^{n+1}}{\Delta z} \quad (1-13)$$

$$b_{a,add}^{n+1} = q_{a,add}^{n+1} + \frac{T_{f,i}^{n+1}}{R_{af}} \quad (1-14)$$

The temperature and pressure in the model can be solved separately in each time step, but it is necessary to update the physical parameters of the drilling fluid to achieve the coupled calculation of wellbore temperature and pressure. The numerical model for the transient distribution of drilling fluid temperature throughout the entire wellbore of a geothermal horizontal well is solved through the following steps, as shown in Fig. 20.

- (1) Input wellbore information (including wellbore trajectory, wellbore structure, and drill string assembly), drilling parameters, and boundary conditions.
- (2) Determine the grid size ΔL and time step Δt
- (3) Use equations (40)–(42) to determine the initial temperature (T_{guess}) and pressure.
- (4) Use equations (30)–(34) to determine the mud physical parameters for each grid under the current temperature and pressure.
- (5) Compute the pressure distribution for each grid.
- (6) Employ equations (1), (1), (2), (2), (3), (3) and (4), auxiliary equations, and boundary conditions to calculate the temperature distribution (T_{pred}) for each grid.
- (7) Determine if the condition $|T_{pred} - T_{guess}| \leq \varepsilon_T$ is satisfied. If not, perform corrective calculations using the current temperature and pressure conditions, returning to step (3) until the condition is met.
- (8) Calculate the unit temperature and pressure for the next time step until the desired time is reached.
- (9) Output temperature distribution data.

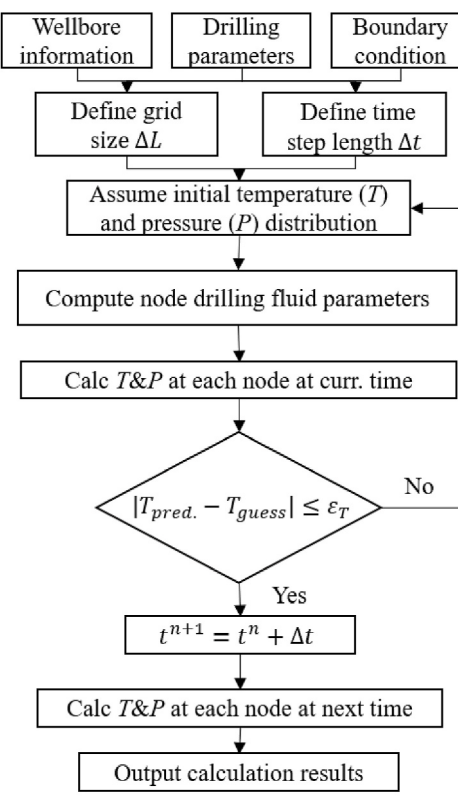


Fig. 20. Flowchart of the solution procedure.

References

- Ando, R., Naganawa, S., 2020. Simulating effect of insulated drillpipe on downhole temperature in supercritical geothermal well drilling. Proceedings of the 42nd New Zealand Geothermal Workshop. Waitangi, New Zealand.
- Angrisani, G., Diglio, G., Sasso, M., et al., 2016. Design of a novel geothermal heating and cooling system: energy and economic analysis. Energy Convers. Manag. 108, 144–159. <https://doi.org/10.1016/j.enconman.2015.11.001>.
- Cao, J., Lye, J., Gonzalez, M., et al., 2024. Exploring the synergy: leveraging oil and gas drilling solutions for enhanced geothermal drilling. In: Proceedings of the 49th

Workshop on Geothermal Reservoir Engineering. Stanford University, Stanford, California. February 12–14.

- Champness, T., Worthen, T., Finger, J., 2008. Development and application of insulated drill pipe for high temperature. High Pressure Drilling. <https://doi.org/10.2172/1001217>.
- Chang, X., Zhou, J., Guo, Y., He, S., Wang, L., Chen, Y., et al., 2018. Heat transfer behaviors in horizontal wells considering the effects of drill pipe rotation, and hydraulic and mechanical frictions during drilling procedures. Energies 11 (9). <https://doi.org/10.3390/en11092414>.
- Chen, Z., Novotny, R.J., 2003. Accurate prediction wellbore transient temperature profile under multiple temperature gradients: finite difference approach and case

- history. SPE Annual Technical Conference and Exhibition. <https://doi.org/10.2118/84583-MS>. All Days.
- Edwardson, M.J., Girner, H.M., Parkison, H.R., Williams, C.D., Matthews, C.S., 1962. Calculation of formation temperature disturbances caused by mud circulation. *J. Petrol. Technol.* 14 (4), 416–426. <https://doi.org/10.2118/124-PA>.
- Espinosa-Paredes, G., Garcia-Gutierrez, A., 2004. Thermal behaviour of geothermal wells using mud and air-water mixtures as drilling fluids. *Energy Conversion and Management - ENERG CONV MANAGE* 45, 1513–1527. <https://doi.org/10.1016/j.enconman.2003.08.023>.
- Espinosa-Paredes, G., Garcia, A., Santoyo, E., Hernandez, I., 2001. TEMLOPI/V.2: a computer program for estimation of fully transient temperatures in geothermal wells during circulation and shut-in. *Comput. Geosci.* 27 (3), 327–344. [https://doi.org/10.1016/S0098-3004\(00\)00102-3](https://doi.org/10.1016/S0098-3004(00)00102-3).
- Farris, R.F., 1941. A practical evaluation of cements for oil wells. *Drilling and Production Practice*.
- Feder, J., 2021. Geothermal well construction: a step change in oil and gas technologies. *J. Petrol. Technol.* 73 (1), 32–35. <https://doi.org/10.2118/0121-0032-JPT>.
- Fénot, M., Bertin, Y., Dorignac, E., Lalizel, G., 2011. A review of heat transfer between concentric rotating cylinders with or without axial flow. *Int. J. Therm. Sci.* 50, 1138–1155.
- Finger, J.T., Jacobson, R.D., Whitlow, G.L., Champness, T., 2000. Insulated Drill Pipe for High-Temperature Drilling.
- Gao, G., Jalali, Y., 2005. Interpretation of distributed temperature data during injection period in horizontal wells. SPE Annual Technical Conference and Exhibition. <https://doi.org/10.2118/96260-MS>. All Days.
- Hasan, A.R., Kabir, C.S., 1994a. Static reservoir temperature determination from transient data after mud circulation. *SPE Drill. Complet.* 9 (1), 17–24. <https://doi.org/10.2118/24085-PA>.
- Hasan, A.R., Kabir, C.S., 1994b. Aspects of wellbore heat transfer during two-phase flow. *SPE Prod. Facil.* 9 (3), 211–216. <https://doi.org/10.2118/22948-PA>.
- Hasan, A.R., Kabir, C.S., 2012. Wellbore heat-transfer modeling and applications. *J. Petrol. Sci. Eng.* 86–87, 127–136. <https://doi.org/10.1016/j.petrol.2012.03.021>.
- Hasan, A.R., Kabir, C.S., Lin, D., 2005. Analytic wellbore-temperature model for transient gas-well testing. *SPE Reservoir Eval. Eng.* 8 (3), 240–247. <https://doi.org/10.2118/84288-PA>.
- Hasan, A.R.R., Izgec, B., Kabir, C.S.S., 2010. Sustaining production by managing annular-pressure buildup. *SPE Prod. Oper.* 25 (2), 195–203. <https://doi.org/10.2118/120778-PA>.
- Hickson, C.J., Kumataka, M., Cotterill, D., Huang, K., 2020. Geothermal drilling and well completions in comparison to oil and gas practices in low temperature (<170°C) sedimentary basin reservoirs. *Geoconvention Virtual Event, September 21-23*.
- Holmes, C.S., Swift, S.C., 1970. Calculation of circulating mud temperatures. *J. Petrol. Technol.* 22 (6), 670–674. <https://doi.org/10.2118/2318-PA>.
- Hu, J., 2017. An improved analytical model for vertical borehole ground heat exchanger with multiple-layer substrates and groundwater flow. *Appl. Energy* 202, 537–549. <https://doi.org/10.1016/j.apenergy.2017.05.152>.
- Kabir, C.S., Hasan, A.R., Kouba, G.E., Ameen, M.M., 1996. Determining circulating fluid temperature in drilling, workover, and well control operations. *SPE Drill. Complet.* 11 (2), 74–79. <https://doi.org/10.2118/24581-PA>.
- Kamel, M.A., Elkhatatny, S., Mysorewala, M.F., Al-Majed, A., Elshafei, M., 2017. Adaptive and real-time optimal control of stick-slip and bit wear in autonomous rotary steerable drilling. *J. Energy Resour. Technol.* 140 (3), 032908 <https://doi.org/10.1115/1.4038131>.
- Kårstad, E., Aadnøy, B.S., 1999. Optimization of mud temperature and fluid models in offshore applications. SPE Offshore Europe Conference and Exhibition. All Days. <https://doi.org/10.2118/56939-MS>.
- Keller, H.H., Couch, E.J., Berry, P.M., 1973. Temperature distribution in circulating mud columns. *Soc. Petrol. Eng. J.* 13 (1), 23–30. <https://doi.org/10.2118/3605-PA>.
- Khaled, M.S., Wang, N., Ashok, P., Oort, E., van, 2023. Downhole heat management for drilling shallow and ultra-deep high enthalpy geothermal wells. *Geothermics* 107, 102604. <https://doi.org/10.1016/j.geothermics.2022.102604>.
- Kutasov, I.M., Caruthers, R.M., Targhi, A.K., Chaaban, H.M., 1988. Prediction of downhole circulating and shut-in temperatures. *Geothermics* 17 (4), 607–618. [https://doi.org/10.1016/0375-6505\(88\)90046-6](https://doi.org/10.1016/0375-6505(88)90046-6).
- Kutlu, B., Takach, N., Ozbayoglu, E.M., Miska, S.Z., Yu, M., Mata, C., 2017. Drilling fluid density and hydraulic drag reduction with glass bubble additives. *J. Energy Resour. Technol.* 139 (4), 042904 <https://doi.org/10.1115/1.4036540>.
- Li, G., Yang, M., Meng, Y., Wen, Z., Wang, Y., Yuan, Z., 2016. Transient heat transfer models of wellbore and formation systems during the drilling process under well kick conditions in the bottom-hole. *Appl. Therm. Eng.* 93, 339–347. <https://doi.org/10.1016/j.applthermaleng.2015.09.110>.
- Liu, W., Gao, K., 2017. Drilling technical difficulties and solutions in development of Hot dry Rock geothermal energy. *Adv. Pet. Explor. Dev* 13, 63–69.
- Ma, T., Chen, P., Zhao, J., 2016. Overview on vertical and directional drilling technologies for the exploration and exploitation of deep petroleum resources. *Geomch. Geophys. Geo-energ. Geo-resour.* 2, 365–395. <https://doi.org/10.1007/s40948-016-0038-y>.
- Mitchell, R.F., Miska, S.Z., 2011. Fundamentals of Drilling Engineering. Society of Petroleum Engineers. <https://doi.org/10.2118/9781555632076>.
- Mohamed, A., Elkhatatny, S.A., Mahmoud, M.A., et al., 2017. The evaluation of micronized barite as a weighting material for completing HPHT wells. Paper Presented at the SPE Middle East Oil & Gas Show and Conference, Manama, Kingdom of Bahrain. <https://doi.org/10.2118/183768-MS>.
- Mohamed, A., Salehi, S., Ahmed, R., 2021. Significance and complications of drilling fluid rheology in geothermal drilling: a review. *Geothermics* 93, 102066. <https://doi.org/10.1016/j.geothermics.2021.102066>.
- Moska, R., Labus, K., Kasza, P., 2021. Hydraulic fracturing in enhanced geothermal systems—field, tectonic and rock mechanics conditions—a review. *Energies* 14 (18), 5725. <https://doi.org/10.3390/en14185725>.
- Nguyen D., Miska S., Yu M., et al. 2010. Modeling thermal effects on wellbore stability. Paper presented at the Trinidad and Tobago Energy Resources Conference, Port of Spain, Trinidad, June 27. doi: <https://doi.org/10.2118/133428-MS>.
- Osinde, N.O., Byiringiro, J.B., Gichane, M.M., et al., 2019. Process modelling of geothermal drilling system using digital twin for real-time monitoring and control. *Designs* 3 (3), 45. <https://doi.org/10.3390/designs3030045>.
- Oueslati H.; Passuello B.; Lehr J.; et al. Learning from the oil & gas industry: leveraging innovation and integration to reduce the risk and cost of geothermal project. Paper Presented at the European Geothermal Congress 2019, Den Haag, The Netherlands, 11–14 June..
- Pastorek, N., Young, K.R., Eustes, A., 2019. Downhole sensors in drilling operations. *Proceedings of the 44th Workshop on Geothermal Reservoir Engineering, Stanford, CA, USA*, pp. 11–13.
- Pimenov, V., Brown, G., Tertychnyi, V., Shandrygin, A., Popov, Y., 2005. Injectivity profiling in horizontal wells through distributed temperature monitoring. SPE Annual Technical Conference and Exhibition. <https://doi.org/10.2118/97023-MS>. All Days.
- Ramey, H.J., 1962. Wellbore heat transmission. *J. Petrol. Technol.* 14 (4), 427–435. <https://doi.org/10.2118/96-PA>.
- Raymond, L.R., 1969. Temperature distribution in a circulating drilling fluid. *J. Petrol. Technol.* 21 (3), 333–341. <https://doi.org/10.2118/2320-PA>.
- Saedi, A.Q.A., Flori, R.E., Kabir, C.S., 2018. New analytical solutions of wellbore fluid temperature profiles during drilling, circulating, and cementing operations. *J. Petrol. Sci. Eng.* 170, 206–217. <https://doi.org/10.1016/j.petrol.2018.06.027>.
- Saedi, A.Q.A., Flori, R.E., Kabir, C.S., 2019. Exploring alteration of near-wellbore geothermal gradient during fluid circulation and production. *J. Petrol. Sci. Eng.* 177, 909–920. <https://doi.org/10.1016/j.petrol.2019.02.013>.
- Song, X., Guan, Z., 2011. Full transient analysis of heat transfer during drilling fluid circulation in deep-water wells. *Acta Petrol. Sin.*, 32 (4): 704.
- Song, X., Li, G., Huang, Z., et al., 2023. Review of high-temperature geothermal drilling and exploitation technologies. *Gondwana Res.* 122, 315–330. <https://doi.org/10.1016/j.gr.2022.10.013>.
- Sui, D., Horpestad, T., Wiktoriski, E., 2018. Comprehensive modeling for temperature distributions of production and geothermal wells. *J. Petrol. Sci. Eng.* 167, 426–446. <https://doi.org/10.1016/j.petrol.2018.03.060>.
- Sun, F., Yao, Y., Chen, M., Li, X., Zhao, L., Meng, Y., et al., 2017. Performance analysis of superheated steam injection for heavy oil recovery and modeling of wellbore heat efficiency. *Energy* 125, 795–804. <https://doi.org/10.1016/j.energy.2017.02.114>.
- Tabatabaei, M., Zhu, D., Hill, A.D.D., 2013. Theoretical basis for interpretation of temperature data during acidizing treatment of horizontal wells. *SPE Prod. Oper.* 28 (2), 168–180. <https://doi.org/10.2118/163138-PA>.
- Tomac, I., Sauter, M., 2017. A review on challenges in the assessment of geomechanical rock performance for deep geothermal reservoir development. *Renew. Sustain. Energy Rev.* 82, 3972–3980. <https://doi.org/10.1016/j.rser.2017.10.076>.
- Trichel, K., Fabian, J., 2011. Understanding and managing bottom hole circulating temperature behavior in horizontal ht wells - a case study based on haynesville horizontal wells. SPE/IADC Drilling Conference and Exhibition. <https://doi.org/10.2118/140332-MS>. All Days.
- Xiao, D., Hu, Y., Wang, Y., Deng, H., Zhang, J., Tang, B., et al., 2022a. Wellbore cooling and heat energy utilization method for deep shale gas horizontal well drilling. *Appl. Therm. Eng.* 213, 118684 <https://doi.org/10.1016/j.applthermaleng.2022.118684>.
- Williamson, H.S., Sawaryn, S.J., 2006. Monte Carlo Techniques Applied to Well Forecasting: Some Pitfalls. *SPE Drill & Compl* 21, 216–227. <https://doi.org/10.2118/89984-PA>.
- Xiao, D., Hu, Y., Meng, Y., et al., 2022b. Research on wellbore temperature control and heat extraction methods while drilling in high-temperature wells. *J. Petrol. Sci. Eng.* 209, 109814 <https://doi.org/10.1016/j.petrol.2021.109814>.
- Yang, M., Zhao, X., Meng, Y., Li, G., Zhang, L., Xu, H., et al., 2017. Determination of transient temperature distribution inside a wellbore considering drill string assembly and casing program. *Appl. Therm. Eng.* 118, 299–314. <https://doi.org/10.1016/j.applthermaleng.2017.02.070>.
- Yang, M., Tang, D., Chen, Y., Li, G., Zhang, X., Meng, Y., 2019. Determining initial formation temperature considering radial temperature gradient and axial thermal conduction of the wellbore fluid. *Applied Thermal Engineering*, 147, , 876–885.
- Yoshida, N., Zhu, D., Hill, A.D.D., 2014. Temperature-prediction model for a horizontal well with multiple fractures in a shale reservoir. *SPE Prod. Oper.* 29 (4), 261–273. <https://doi.org/10.2118/166241-PA>.
- Yoshioka, K., Zhu, D., Hill, A.D., Dawkratjai, P., Lake, L.W., 2007. Prediction of temperature changes caused by water or gas entry into a horizontal well. *SPE Prod. Oper.* 22 (4), 425–433. <https://doi.org/10.2118/100209-PA>.
- Zhang, Z., Xiong, Y., Mao, L., Lu, J., Wang, M., Peng, G., 2019. Transient temperature prediction models of wellbore and formation in well-kick condition during circulation stage. *J. Petrol. Sci. Eng.* 175, 266–279. <https://doi.org/10.1016/j.petrol.2018.12.044>.
- Ziabakhsh-Ganji, Z., Nick, H.M., Donselaar, M.E., Bruhn, D.F., 2018. Synergy potential for oil and geothermal energy exploitation. *Appl. Energy* 212, 1433–1447. <https://doi.org/10.1016/j.apenergy.2017.12.113>.